This document was prepared in conjunction with work accomplished under Contract No. AT(07-2)-1 with the U.S. Department of Energy.

DISCLAIMER

TA 862

TECHNICAL DIVISION
SAVANNAH RIVER LABORATORY

DPST-65-197

CC: T. C. Evans - H. C. Minton, Jr., SRP
W. P. Overbeck - A. A. Johnson, SRL
J. W. Morris
R. T. Huntoon - W. R. McDonell
C. L. Angerman
M. R. Louthan, Jr.
TIS File Copy
Vital Records File

M E M O R A N D U M

March 8, 1965

TO: P. H. PERMAR

FROM: G. R. CASKEY, JR.
G. R. Caskey, Jr./c.l.a.

MECHANICAL PROPERTIES OF URANIUM ALLOYS

INTRODUCTION

Cavitational swelling in uranium-base fuel has been attributed to boundary sliding arising from internal stresses due to anisotropic growth.(1) Large cavities or holes (10-200 microns) form preferentially along boundaries or at intersections of boundaries. This mode of swelling occurs at intermediate temperatures, 375-550°C, after exposures have exceeded threshold values which are dependent on alloy composition.

The mechanical properties of uranium-base alloys might be expected to correlate with their swelling susceptibility. Room-temperature tensile tests were made on a series of alloys to explore the possibility of such a relation and isolate the specific properties of major importance. This memorandum presents the results of the tensile tests. Correlations of these results with swelling susceptibility will be made in later reports of the irradiation behavior of the fuel materials.

SUMMARY

Room-temperature mechanical properties were determined for dingot- and ingot-base uranium alloys containing Fe, Si, Al, and Mo. The principal effects of alloy additions on the mechanical properties of beta-treated (oil-quenched) materials were as follows:

- As iron, silicon, and aluminum additions increased in:

Dingot-Base Alloys (50 ppm C)	Ingot-Base Alloys (500 ppm C)
Yield strength increased	Yield strength increased
Ductility decreased	Ductility decreased slightly
Fracture strength unaffected	Fracture strength increased, noticeably in higher alloys*

* The difference in the effect on fracture strength between ingot- and dingot-base alloys may be related to differences in crack nucleation and propagation in the two groups of materials.

- There was little difference in deformation mechanisms attributable to difference in carbon content between dingot (50 ppm C) and ingot (500 ppm C) alloys.
- Molybdenum additions increased both ductility and fracture strength of the alloys. The yield strength was not altered.
- Alpha annealing increased the ductility and strain-hardening exponent, and decreased the yield strength of the alloys. These changes were due to relief of residual stresses that arose during heat treatment and machining.
- Thermal cycling from room temperature to 630°C weakened low-alloy ingot uranium and decreased its ductility from 8 to 2%. Cold working prior to the thermal cycling lessened these effects.

DISCUSSION

Alloy compositions representing a wide range of resistance to cavitational swelling during irradiation were selected for the mechanical tests. The alloys are listed in Table I. Unalloyed dingot uranium (993) is the highest purity uranium commercially available, and forms the base for one series of alloys. Unalloyed ingot metal contains about 500 ppm C as the principal impurity and forms the base for the second series of alloys.

The distribution of the alloy constituents within the microstructure of the alloys as determined by the prior history, as for example the heat treatment, has a significant influence upon mechanical behavior. Consequently, most of the mechanical tests were performed on samples in the beta-treated, oil-quenched condition, the standard heat treatment used for fuel elements. When heat treated in this manner, there is some fraction of the alloying addition present in a non-equilibrium condition within some of the alloys. A limited number of the alloys were also tested after alpha annealing.

"Button-end" tensile specimens of 1/8-inch diameter with a 1/2-inch gage length were tested in tension at room temperature at a loading rate of 250 lb/min. Load-extension curves were recorded autographically up to a strain of 4%, the limit of the extensometer. Original and final gage diameters were measured. Selected points from the load-extension record were converted to true stress and true plastic strain and plotted as shown in Figures 1 to 16. In several cases conventional enginering stress-strain curves were also prepared. Each curve represents data from the testing of a single specimen unless otherwise stated.

Mechanical properties (Table II) obtained from the test data were:

Property	Method of Measurement
Modulus of elasticity (E)	Slope of the initial (approximately straight) portion of curve
Yield strength ($YS_{0.2}$)	Engineering stress at 0.2% offset
Tensile strength (UTS)	Nominal stress at maximum load
Reduction in area (RA)	Percent change in area, $\Delta A/A_o$
Proportional limit (σ_y)	True stress at point of departure of curve from straight line
Fracture strength (σ_f)	True stress at fracture
Strain to fracture (ϵ_f)	Total strain at fracture
Strain-hardening exponent (n)	Exponent in the relation $\sigma = k\epsilon^n$ where σ = true stress for range of ϵ from 0.001 to 0.01 and ϵ_p = true plastic strain
Strength coefficient (k)	Coefficient of ϵ_p in above relation

Both deformed and fractured specimens were examined metallographically for twins, cracks, and other features related either to deformation or fracture. Replicas of the fractured faces of the specimens were also examined with the electron microscope.

Properties of Dingot-Base Alloys

The base composition for determining the effects of alloying was unalloyed dingot uranium which is the highest purity uranium that is normally available for reactor use. The properties of this material are listed in Table II. Engineering stress-strain curves of several specimens extended differing amounts are shown in Figure 17. Differences between the stress-strain curves are small, even though none of the specimens was annealed prior to testing.

Figure 18, which compares stress-strain curves for as-machined and annealed specimens, demonstrates that there is some degree of hardening present in the as-machined (beta-treated) specimens. In addition to machining, the beta treatment and oil quench probably also account for part of the observed hardening.

Comparison of the mechanical properties of the alloyed with the unalloyed dingot uranium (Table II) indicates that iron, silicon, and aluminum additions raise the proportional limit (σ_y) but have essentially no effect on the fracture strength (σ_f). Ductility and the strain-hardening exponent are reduced by alloying and the strength coefficient (k) is increased by additions of iron and aluminum but is decreased by the addition of iron and silicon. The effect of these alloying additions then is primarily upon those structural changes that influence the initiation of twinning and slip and not upon the conditions that govern fracture.

In all cases fracture occurred at the maximum load without any measurable necking of the specimens prior to fracture. This effect is also manifested in the fact that the strain-hardening exponent is greater than the strain at fracture. In the analysis of the stress-strain curve by Lubahn,[2] it is shown that for metals that conform to the relationship $\sigma = k\epsilon^n$, the condition for the maximum in the stress-strain curve leads to the result that the strain at this maximum is numerically equal to the strain-hardening exponent. Since it is generally believed that a state of triaxial tension exists in the necked region of a tensile specimens, the lack of necking in uranium implies that such a stress state almost immediately initiates fracture within the uranium. The low ductility of uranium at room temperature is then due to the inability of the uranium to deform under a triaxial stress state without cracking. At higher temperatures uranium does neck down prior to fracture, so that this type of behavior appears to be associated with room-temperature deformation.

Properties of Ingot-Base Alloys

Effect of Alloying

Table II also compares the mechanical properties of several ingot-base alloys. Four of these are low alloys of slightly differing iron and silicon contents, the others are intermediate or high alloys based primarily upon the addition of either 350 or 800 ppm silicon with iron, aluminum, or molybdenum additions.

The five unalloyed and low alloy ingot base cores showed greater variations in some mechanical properties than would be expected. Alloys 33382 and 92794 which have nearly the same composition show large differences in ductility, elastic modulus, proportional limit, strain-hardening exponent, and strength coefficient. Yield, tensile, and fracture strengths are similar, on the other hand. Although the compositions are similar, there is a pronounced difference in the Fe/Si ratio, which is 4 for 33382 and 2.5 for 92794. This factor may influence the manner of distribution of the iron and silicon within the alloys and hence alter their properties.

The higher alloy additions are best examined by beginning with the U-Si alloys of 350 and 800 ppm silicon. Addition of silicon increases all of the properties except ductility which decreased from 9.0% for unalloyed ingot to 8.1% for U-350 ppm Si, to 4.9% for U-800 ppm Si. The strengthening associated with the silicon addition was more pronounced for the yield strength than for tensile strength at the 350 ppm level. With addition of 800 ppm Si both yield and tensile strengths were increased. The addition of either iron and aluminum to the U-350 ppm Si alloy caused a further increase in strength (YS, UTS, σ_y, and σ_f). Iron and aluminum appear to be opposite in their influence on ductility and strain hardening; iron decreases ductility and increases n and k whereas aluminum has little effect on ductility but decreases n and k. The simultaneous addition of iron and aluminum to a U-250 ppm Si alloy yielded an alloy with properties similar to those of the U-350 ppm Si alloy except for lower values of n and k. The addition of 1000 Mo to U-350 ppm Si lowered the yield strength and proportional limit only slightly, but had a pronounced effect in increasing the ultimate

strength and ductility, as well as n and k.

The one high alloy that was free of large silicon additions was 98359 which contained 300 ppm Fe and 900 ppm Al. This alloy had mechanical properties roughly comparable to those of the Fe-Si-Al alloy (XM2) of comparable total alloy content (about 800 ppm). Values of n and k were higher for the Fe-Al alloy than for the Fe-Si-Al alloy, but the strengths and ductility were about the same.

Several general features of the influence of alloying on mechanical properties are evident:

- The only alloy addition that significantly improved ductility was molybdenum. All others (Fe, Si, Al) reduced ductility as compared to unalloyed ingot uranium.
- With one or two exceptions, the alloys had about the same fracture strengths (or tensile strengths) and ductility, although there were differences in YS, σ_y, n, and k. This implies that variations in alloying affect plastic deformation more than they affect fracture.
- For uranium containing small alloy additions, the difference in carbon content between dingot (50 ppm) and ingot (500 ppm) base uranium had little effect on the mechanical properties.
- Correlation of property changes with alterations in level of individual alloying elements is of doubtful validity in view of the small sampling available, except for the case of Si as described above.

Effect of Annealing

Prolonged annealing in the high alpha region (400-600°C) had a pronounced effect on the properties of both ingot- and dingot-base unalloyed and low-alloy uranium (Table III and Figures 19 through 23). The principal effects were to improve ductility and increase the strain-hardening exponent, except for 92794 where the exponent decreased. Tensile or fracture strengths increased sometimes (33384 and 92794) or decreased (993, 927, and 92754). The yield strengths decreased.

In the case of the unalloyed dingot uranium, these property changes produced by annealing can be interpreted as arising from the relief of internal stresses introduced by beta treatment and machining. In this case those properties sensitive to the state of internal stress (YS, σ_y, and n) were altered, but those properties associated with the fracture process (UTS, σ_f, and k) were not changed very much.

In the ingot-base uranium and the low-alloy dingot, interpretation of the property changes that accompany annealing require consideration of microstructural changes that might attend precipitation of phases such as U_3Si, U_6Fe, UC, or UAl_2, or segregation of the alloy elements to preferred sites. The data are not extensive or certain enough, however, to draw any significant conclusions. Detailed

metallographic examination, including transmission electron microscopy would aid such interpretation.

Effect of Thermal Cycling

Thermal cycling between room temperature and 500°C produced cavities similar, in their early stage of formation, to those produced during irradiation.(3) The effect of such treatment on the mechanical properties of low-alloy ingot uranium is shown in Figure 24. Two specimens, one as-machined and one cold-worked (prestrained 1%), were cycled from room temperature to 630°C for 4 hours, the cycle being 1 minute in the furnace and 1 minute out. Thermal cycling weakened the metal as would be expected and lowered the ductility of the as-machined specimen to about 2%. The specimen that was cold worked prior to thermal cycling appeared more resistant to the weakening effects of cycling than the as-machined specimen. Its properties were similar to those of the alpha-annealed (100 hours at 400°C) specimens. Since the specimens were not run in duplicate, the structure of the alloy in the thermal cycled condition is not known.

Microstructural Features of Deformation

The course of deformation in the unalloyed dingot uranium was accompanied by an increase in the volume fraction of twins and in the total amount of internal boundary per unit area, Table IV and Figures 25 and 26. As deformation proceeded the ratio of fraction of twins to reduction in area decreased, indicating that twinning contributed relatively less and slip relatively more to the deformation as the deformation increased. Subgrain boundaries in those areas relatively free of twins were counted separately. On the basis of these counts, there was apparently a decrease in the subgrain surface to volume ratio or an increase in subgrain size during deformation. This is contrary to the expected decrease in subgrain size usually observed in cold working and implies that there is considerable subgrain boundary mobility in unalloyed dingot uranium at room temperature.

Fractographic Studies

Examination of fractured specimens revealed features of distinction and similarity among the alloys, Table V. The general fracture surfaces were commonly approximately perpendicular to the tensile axis and were jagged on a fine scale (Figure 27a) except for the alloy containing 1000 ppm molybdenum where the fracture had more of a scalloped character. Secondary cracks (cracks other than those associated with the primary fracture) were observed in all of the alloys except the U-350 ppm Si and U-350 ppm Si-1000 ppm Mo alloys. Such cracks were most prevalent near the fracture face but also appeared throughout the gage section from surface to center. In cases where the fracture path was discernible, the cracks most commonly lay along grain boundaries (Figure 27b). In the U-Si-Al alloy, a crack (apparently transgranular) was observed that was almost perpendicular to the fracture and which was surrounded by heavily twinned metal (Figure 28).

The specimens of unalloyed dingot uranium showed two rather unique features: a double fracture (Figure 29a) and transverse grain boundary cracks emanating from the points of intersection of a deformation band with the grain boundaries (Figure 29b).

Previous fractographic studies of uranium-base alloys had shown that fracture was initiated at second-phase particles, predominantly UC, and that the fracture path was determined by second-phase distributions.[4,5] In contrast, the present work showed that carbon contents between 50 and 500 ppm had little effect on the fracture strength. In addition, optical metallography did not reveal any apparent association of the fracture path with second-phase precipitates. To further elucidate the role of second-phase particles in the fracture processes, cellulose acetate-carbon replicas of the fracture surfaces of several different ingot- and dingot-base alloys, Table V, were prepared and examined with the electron microscope.

The fracture path was predominantly transgranular and only limited evidence of an association of second-phase particles with fracture was observed. Three types of transgranular fracture were apparent in most samples: (1) fibrous fracture, characteristic of ductile fracture processes, Figure 30a, (2) stair-step cleavage fracture (probably associated with the slip planes[2]) Figure 30b, and (3) "river" patterns, characteristic of classical cleavage, Figure 30c. The amount of fibrous fracture increased with increasing strain to fracture, regardless of the alloy type or composition. The two extremes in fracture appearance were the alloy containing 800 ppm Si, which failed almost entirely by brittle processes, and the 1000 ppm Mo alloy, which failed almost entirely by fibrous fracture processes. Limited evidence of intergranular fracture was found in several of the alloys; however, evidence of secondary cracks along grain boundaries was quite common. The mode of fracture changed from grain to grain within a sample illustrating a relation between grain orientation and fracture process.

Twinning played a predominant role in room-temperature deformation instead of carbides and other second-phase precipitates. Crack initiation by twin intersection occurred frequently, as shown in Figure 31. At elevated temperatures slip should play a more important role in the deformation process and the role of carbides and grain boundary sliding in crack nucleation at these temperatures cannot be predicted from room-temperature tests. Therefore, direct comparison of the room-temperature fracture characteristics and the behavior of the alloys during irradiation at elevated temperatures should not be made.

REFERENCES

1. Caskey, G. R., Jr. and C. L. Angerman. Swelling of Thick-Walled Tubular Fuel Elements of Unalloyed Uranium. DP-828 (Secret).

2. Lubahan, J. D. "Deformation Properties," Materials Engineering Design for High Temperatures. J. Marin, ed., Pennsylvania State University (1958).

3. Angerman, C. L. and M. R. Louthan, Jr. "Mechanical Cavitation of Unirradiated Uranium." DPST-64-362 (Secret).

4. Foster, E. L., Jr. A Study of the Tensile Fracture and Microstructure of Uranium. BMI-1664, February 1964.

5. Bierlein, T. K. and B. Mastel. Fractography of Some Reactor Fuel Materials. HW-57207, August 1958.

GRC:bdp

TABLE I

CHEMICAL ANALYSES OF ALLOYS

Ingot Number	Alloy Code	Composition, ppm C	Fe	Si	Al	Mo	(Fe+Si)	Ratio Fe/Si
993	Dingot	28	57	11	32	-	68	5.20
882)	Low	25	150	90	24	-	240	1.67
927)	alloy	32	150	110	24	-	260	1.36
2122)	dingot	24	140	110	24	-	250	1.27
3260	UK	28	300	30	890	-	330	10
33382	Ingot	420	105	26	<6	-	131	4.04
33384)	Low	428	137	88	<6	-	225	1.56
92754)	alloy	542	128	58	7	-	186	2.21
92794)	ingot	540	97	39	<6	-	136	2.49
98341)		599	151	89	9	-	240	1.70
98359	UK	484	333	76	949	-	409	4.38
98464	XC2	544	287	361	<6	-	648	0.8
98483	XD2	416	63	310	778	-	373	0.02
98470	XG2	477	75	325	<6	-	400	0.23
98479	XM2	411	289	222	274	-	511	1.30
98727	XW2	468	98	327	<6	1000	425	0.3
SA4	XH2	500	53	718	86	-	771	0.07

TABLE II

MECHANICAL PROPERTIES OF URANIUM ALLOYS

Ingot Number	Alloy Code	E, mpsi	YS, kpsi	UTS, kpsi	RA, %	σ_y, kpsi	σ_f, kpsi	n	k, kpsi
Dingot Base									
993	Unalloyed	29.9	38.9	91.1	8.9	16.1	100.0	0.230	165
882	Low alloy	11.3	46.5	98.5	4.1	28.3	102.8	0.151	151
2122	"	18.7	45.5	89.0	5.6	25.5	94.5	0.181	112
3260	UK	22.7	56.2	97.0	4.5	26.6	101.5	0.176	216
Ingot Base									
33382	Unalloyed	17.3	41.6	90.2	9.0	22.4	100.0	0.184	135
92794	Low alloy	21.8	44.8	94.0	5.7	18.6	99.7	0.221	177
92754	"	27.5	49.0	106.0	8.1	21.1	115.0	0.212	186
33384	"	30.5	48.8	93.0	4.9	31.7	98.0	0.160	139
98341	"	18.7	48.2	97.0	6.2	24.7	103.5	0.225	198
98359	UK	20.7	54.6	99.2	7.3	32.5	107.0	0.211	206
98464	XC2	16.5	48.0	97.5	7.2	20.0	105.7	0.255	233
98479	XM2	16.2	50.8	93.0	7.3	26.4	101.0	0.179	155
98470	XG2	25.4	46.8	91.0	8.1	22.4	99.2	0.220	187
98483	XD2	28.3	51.6	102.0	8.1	34.3	111.0	0.162	146
98727	XW2	26.5	42.0	110.0	11.2	18.0	126.5	0.282	242
SA4	XH2	29.0	56.5	120.0	4.9	26.4	126.0	0.252	268

TABLE III

EFFECT OF ALPHA ANNEAL ON MECHANICAL PROPERTIES

Ingot Number		E, mpsi	YS, kpsi	UTS, kpsi	RA, %	σ_y, kpsi	σ_f, kpsi	n	k, kpsi
993	β	29.9	39	91	8.9	16	100	0.230	165
993	α*	14	30	92	(9.8)	12	(96)	0.279	168
882	β	11.3	46	98	4.1	28	103	0.151	151
927	α**	11.3	38	68	-	17	71	0.230	145
92794	β	21.8	45	94	5.7	19	100	0.221	177
92794	α*	21.8	47	98	(7.9)	26	(102)	0.192	163
92754	β	27.5	49	106	8.1	21	115	0.212	186
92754	α*	27.9	46	95	(6.2)	17	(98)	0.214	175
33384	β	30.5	49	93	4.9	32	98	0.160	139
33384	α*	38.6	36	98	11.8	16	111	0.278	198

* 100 hours at 400°C.
** Anneal 48 hours at 600°C.
() Estimated values.

TABLE IV

MICROSTRUCTURAL CHANGES DURING DEFORMATION
UNALLOYED DINGOT URANIUM (993)

Total Extension, %	Reduction in Area, %	Volume Fraction Twins, f_v	Surface-Volume Ratio, S_v, mm^2/mm^3	
			Subgrain Only*	All Boundaries
0	0	0.071	-	147
0.9	0.6	0.114	95.4	185
2.5	2.1	0.197	81.2	254
5.0	4.6	0.237	64.4	337
10.2	8.9	0.298	57.7	353

TABLE V

MICROSCOPIC OBSERVATION OF FRACTURED SPECIMENS*

Alloy	Dingot, Ingot Number	Volume Fraction Twins, f_v	Reduction in Area, %	f_v/RA	Secondary Cracks
Unalloyed dingot	993	0.30	8.9	0.024	
Low alloy dingot	2122	0.27	5.6	0.048	Many
Dingot-Fe-Si	3260	0.27	4.5	0.060	Several
Unalloyed dingot	33382	0.26	9.0	0.029	Several
Low alloy ingot	98341	0.28	6.2	0.045	Several
Ingot-350 Si	98470	0.23	8.1	0.028	None
Ingot-350 Si-800 Al	98483	0.28	8.1	0.035	Several
Ingot-250 Fe-350 Si	98464	0.22	7.2	0.031	Few
Ingot-350 Si-1000 Mo	98727	0.31	11.2	0.028	None
Ingot-350 Fe-800 Al	98359	0.23	7.3	0.032	Many
Ingot-250 Fe-200 Si-250 Al	98479	0.26	7.3	0.036	Several
Ingot-800 Si-	SA4	0.28	4.9	0.057	

* The fracture surfaces of these specimens were also examined with the electron microscope.

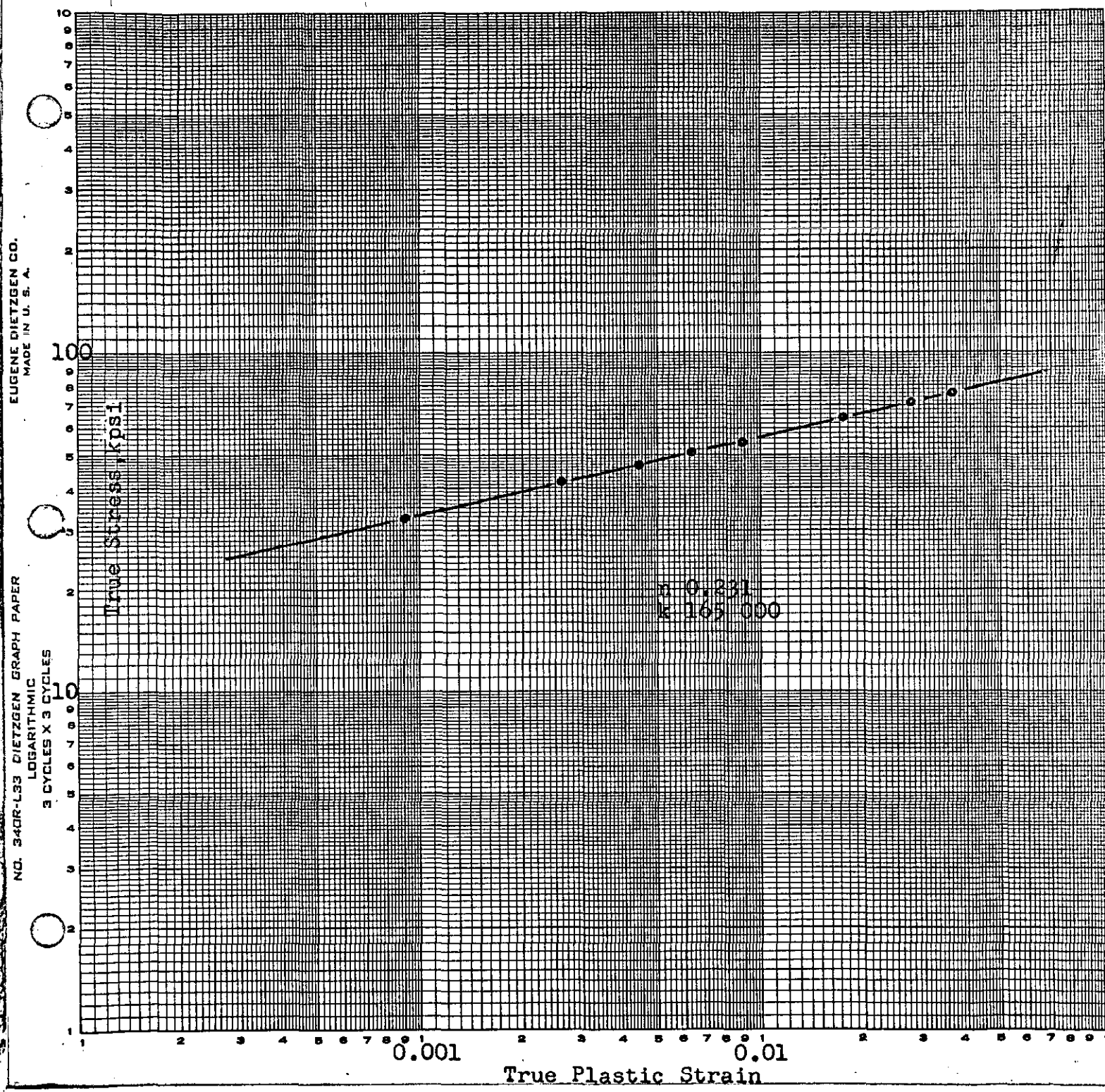

FIGURE 1. TRUE STRESS-TRUE STRAIN BEHAVIOR OF DINGOT 993
U-57 ppm Fe-11 ppm Si-32 ppm Al

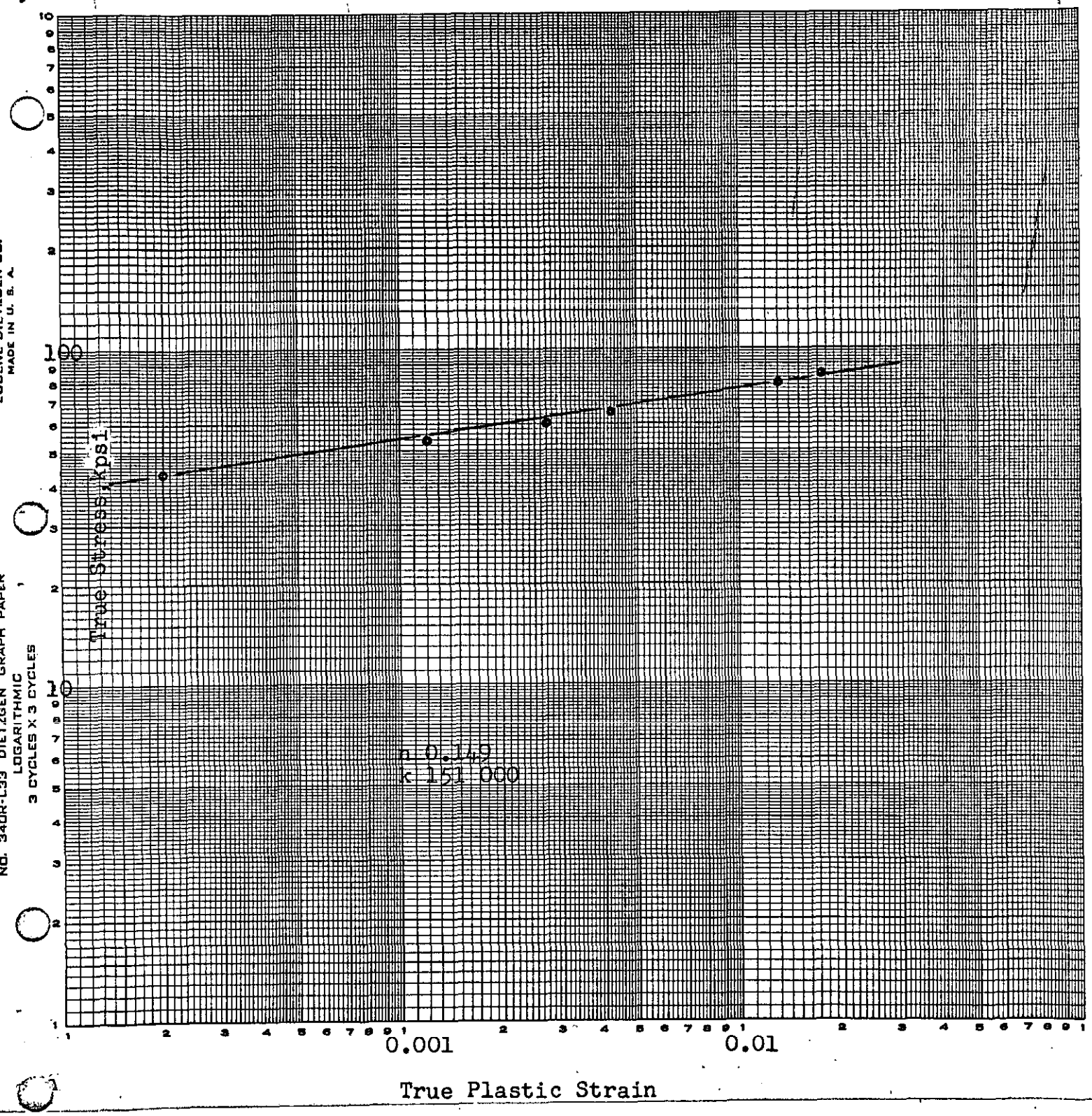

FIGURE 2. TRUE STRESS-TRUE STRAIN BEHAVIOR OF DINGOT 882
U-150 ppm Fe-90 ppm Si-24 ppm Al

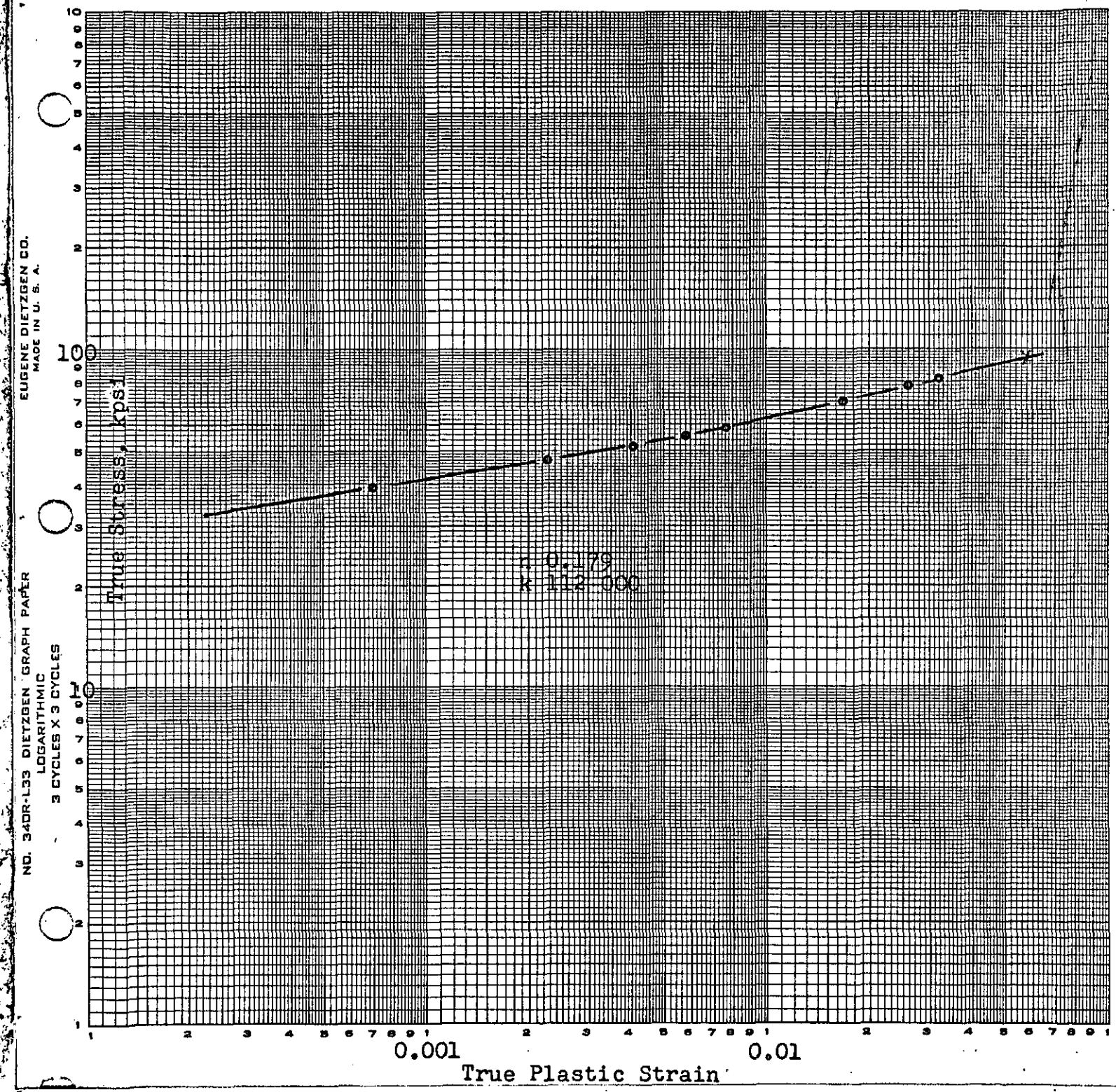

FIGURE 3. TRUE STRESS-TRUE STRAIN BEHAVIOR OF DINGOT 2122
U-140 ppm Fe-110 ppm Si-24 ppm Al

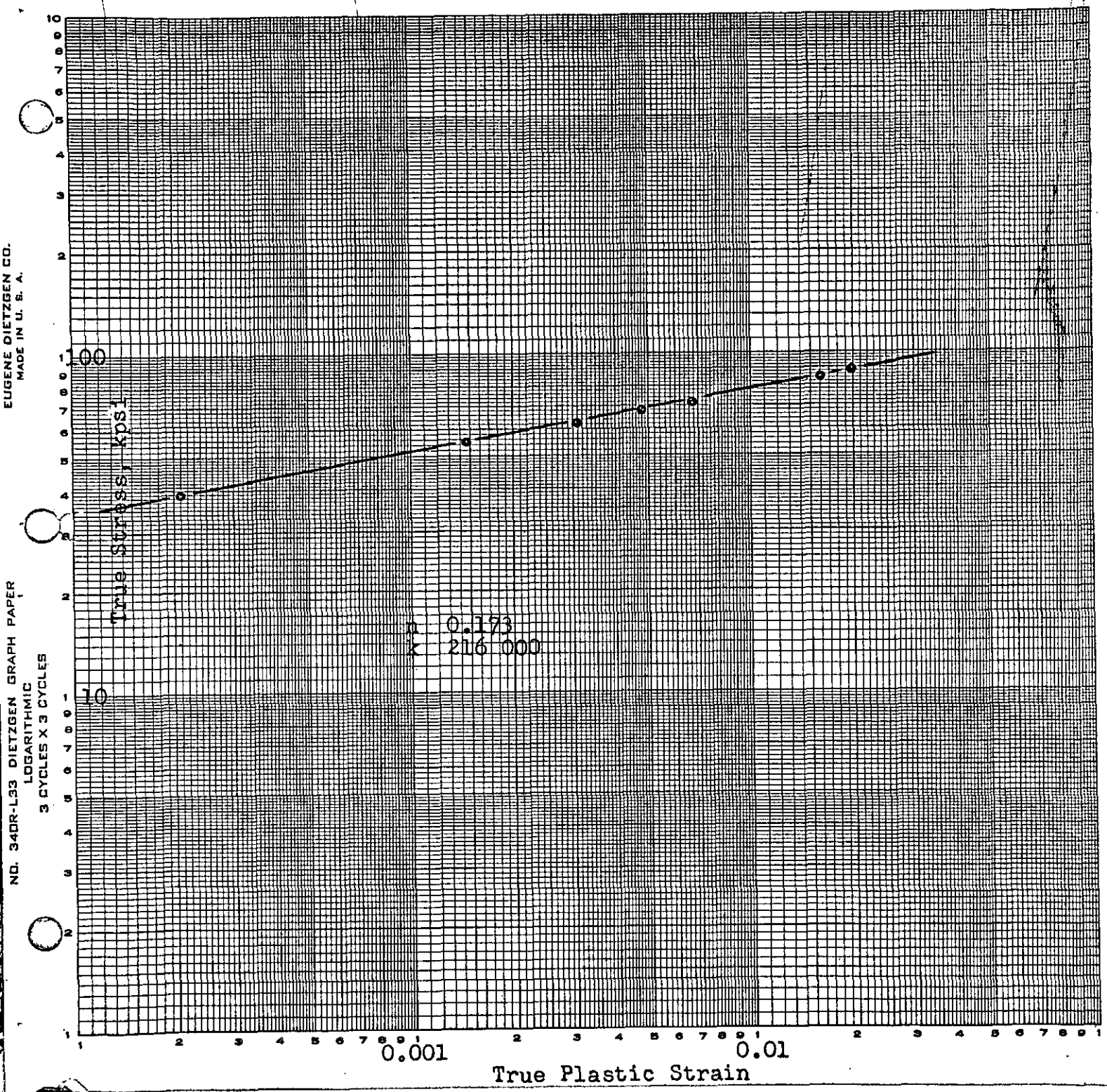

FIGURE 4. TRUE STRESS-TRUE STRAIN BEHAVIOR OF DINGOT 3260
U-300 ppm Fe-30 ppm Si-890 ppm Al

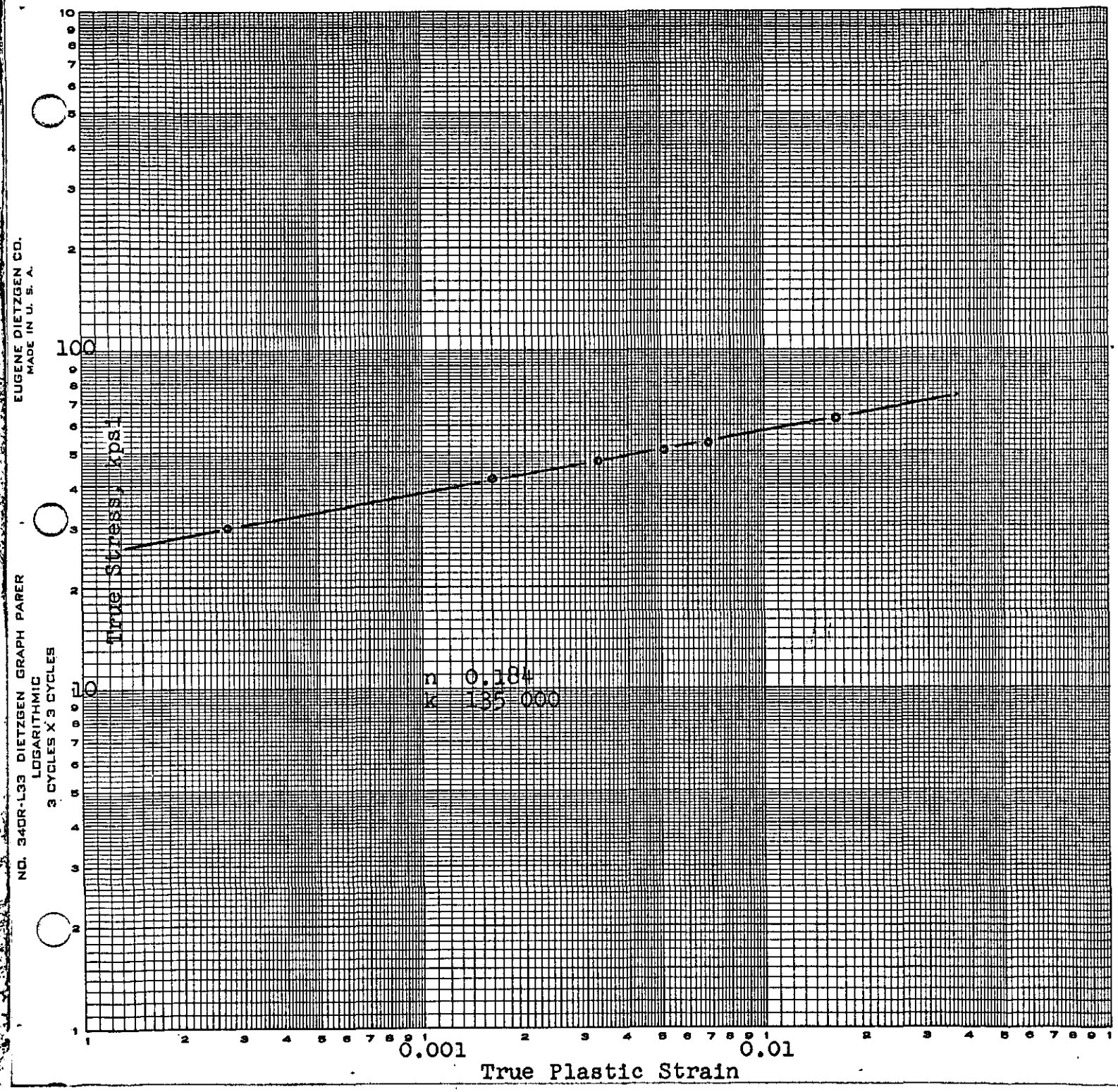

FIGURE 5. TRUE STRESS-TRUE STRAIN BEHAVIOR OF INGOT 33382
U-105 ppm Fe-25 ppm Si-<6 ppm Al

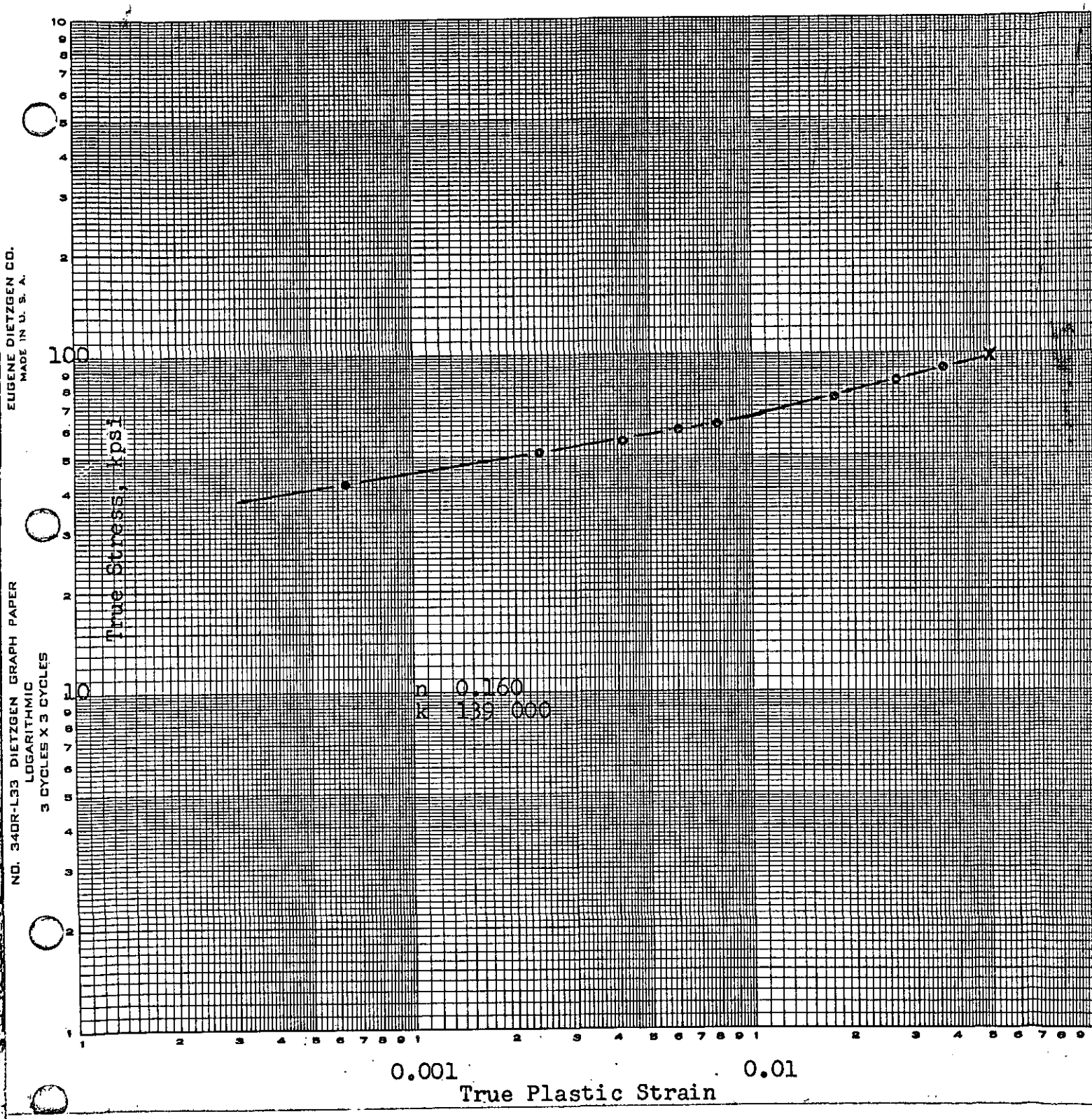

FIGURE 6. TRUE STRESS-TRUE STRAIN BEHAVIOR OF INGOT 33384
U-137 ppm Fe-88 ppm Si-<6 ppm Al

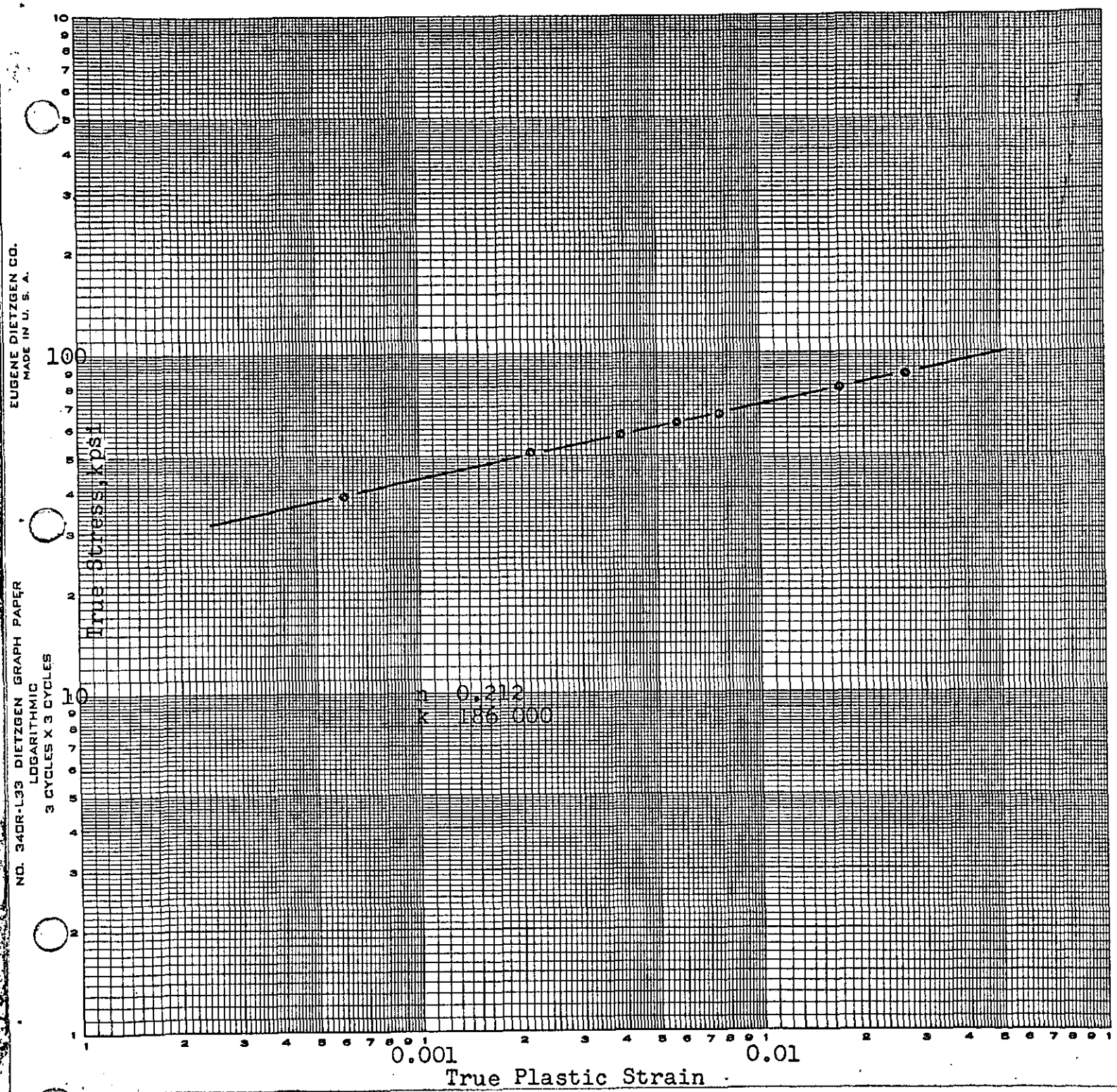

FIGURE 7. TRUE STRESS-TRUE STRAIN BEHAVIOR OF INGOT 92754
U-128 ppm Fe-58 ppm Si-7 ppm Al

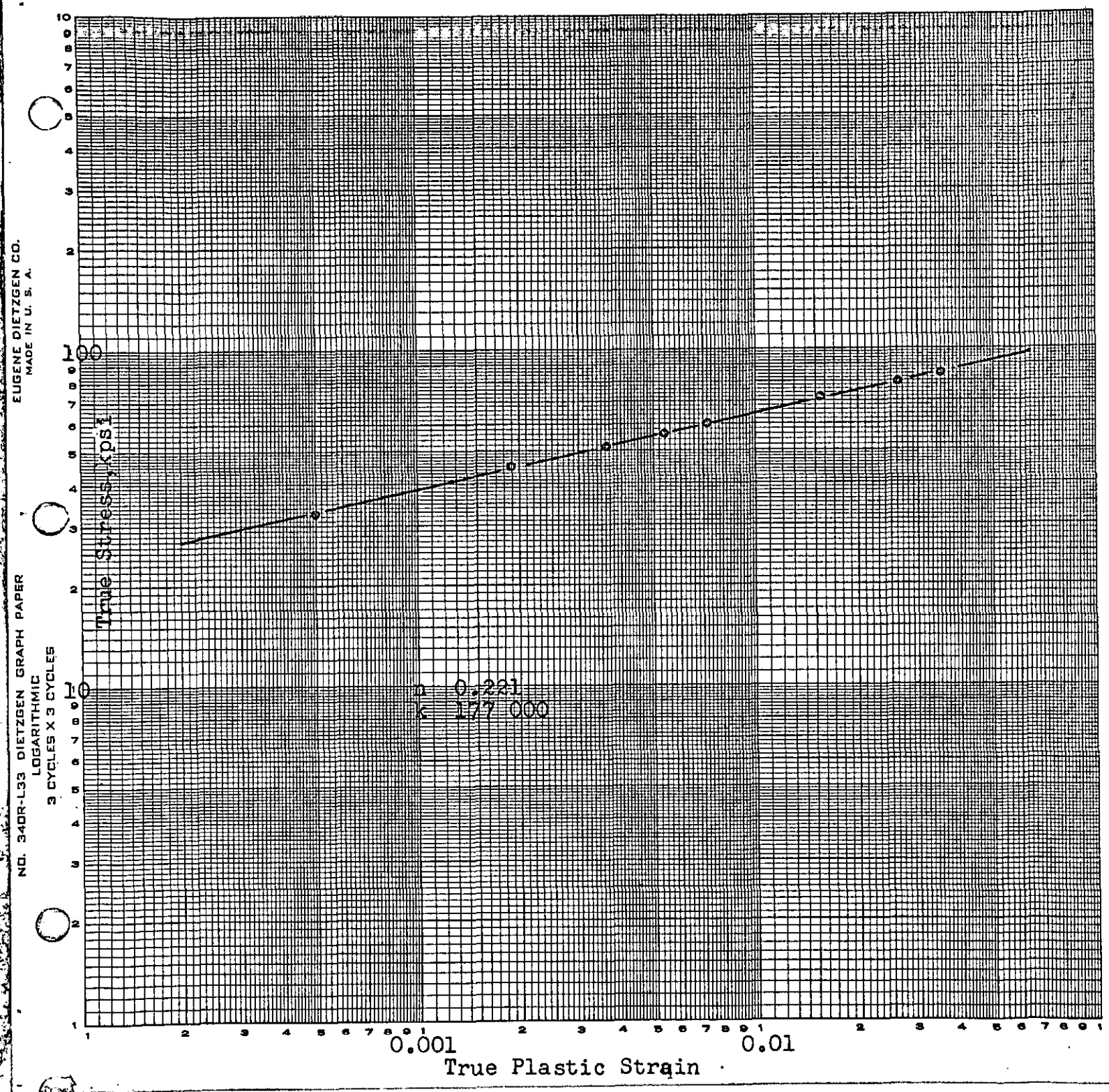

FIGURE 8. TRUE STRESS-TRUE STRAIN BEHAVIOR OF INGOT 92794(16B)
U-97 ppm Fe-39 ppm Si-<6 ppm Al

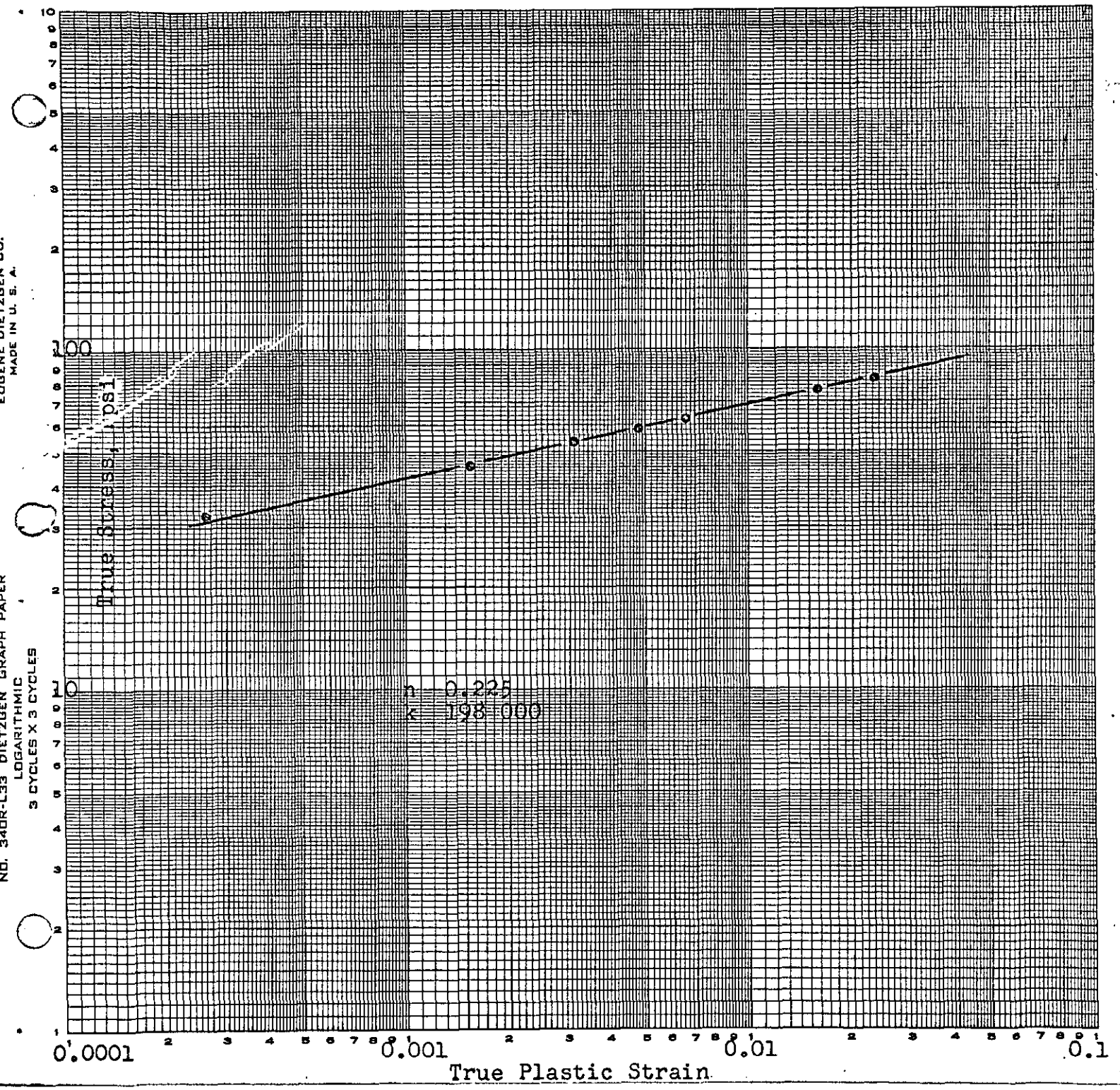

FIGURE 9. TRUE STRESS-TRUE STRAIN BEHAVIOR OF INGOT 98341
U-151 ppm Fe-89 ppm Si-9 ppm Al

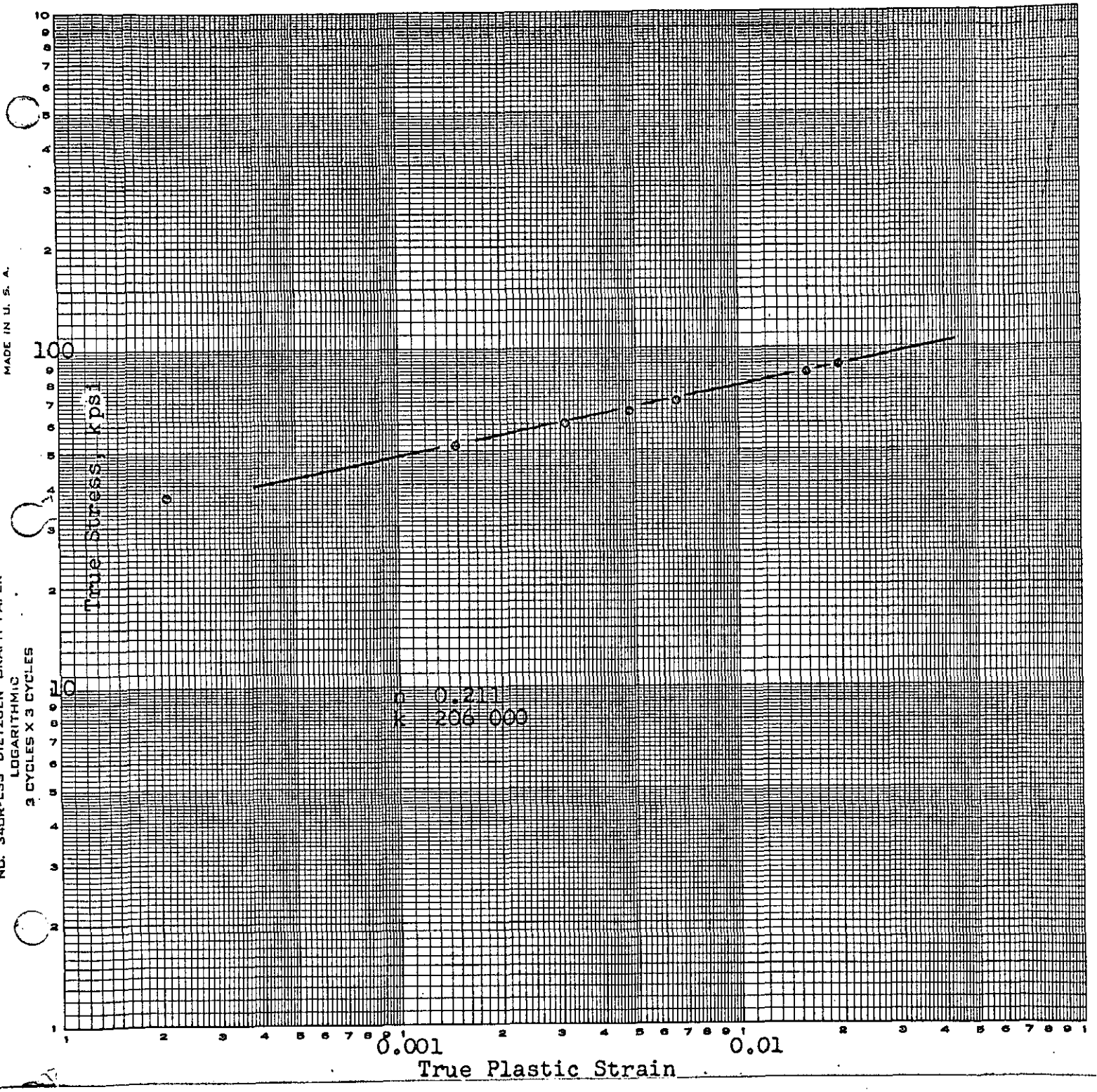

FIGURE 10. TRUE STRESS-TRUE STRAIN BEHAVIOR OF INGOT 98359
U-333 ppm Fe-76 ppm Si-949 ppm Al

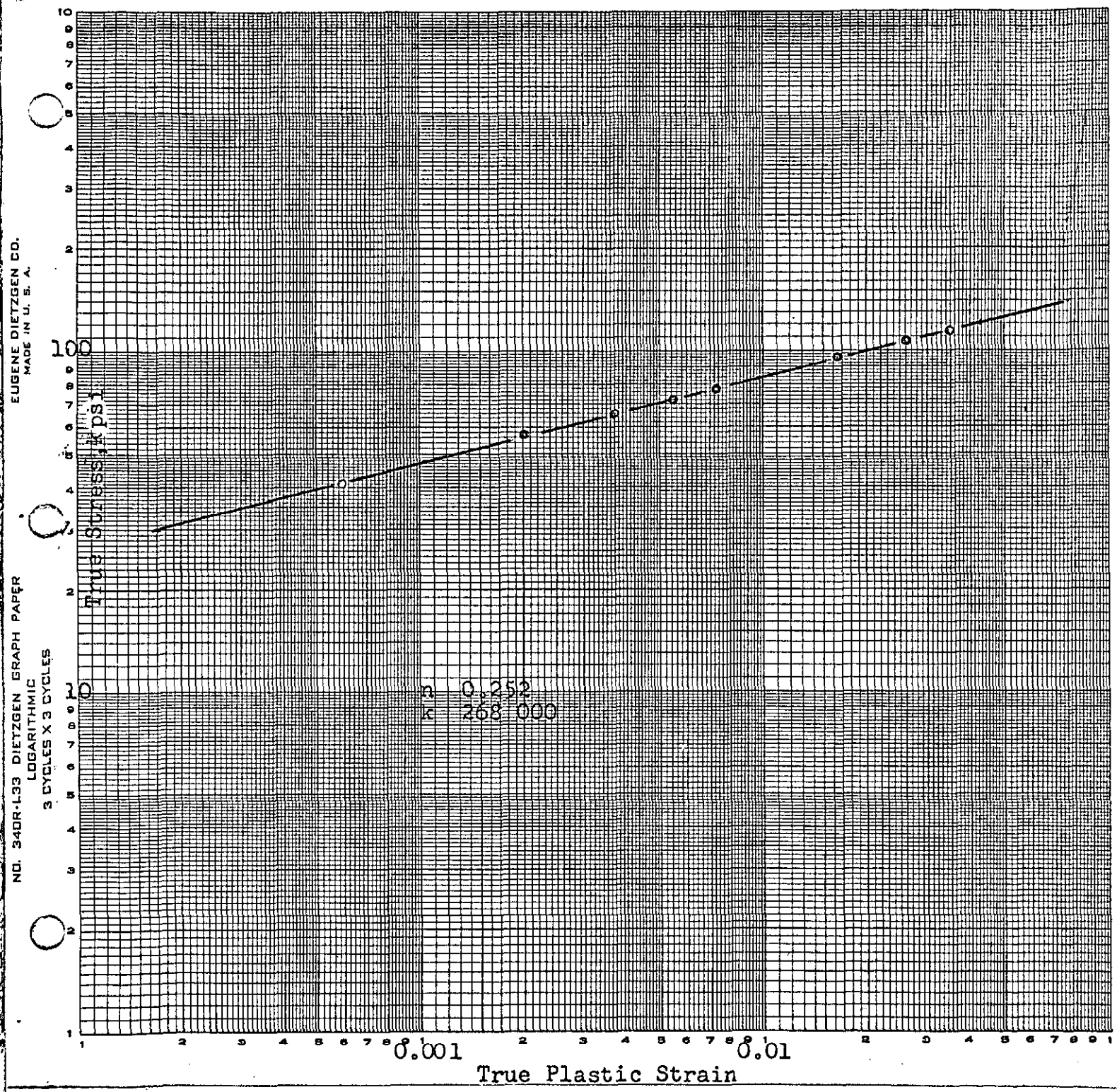

FIGURE 11. TRUE STRESS-TRUE STRAIN BEHAVIOR OF INGOT SA4 (3H)
U-53 ppm Fe-718 ppm Si-86 ppm Al

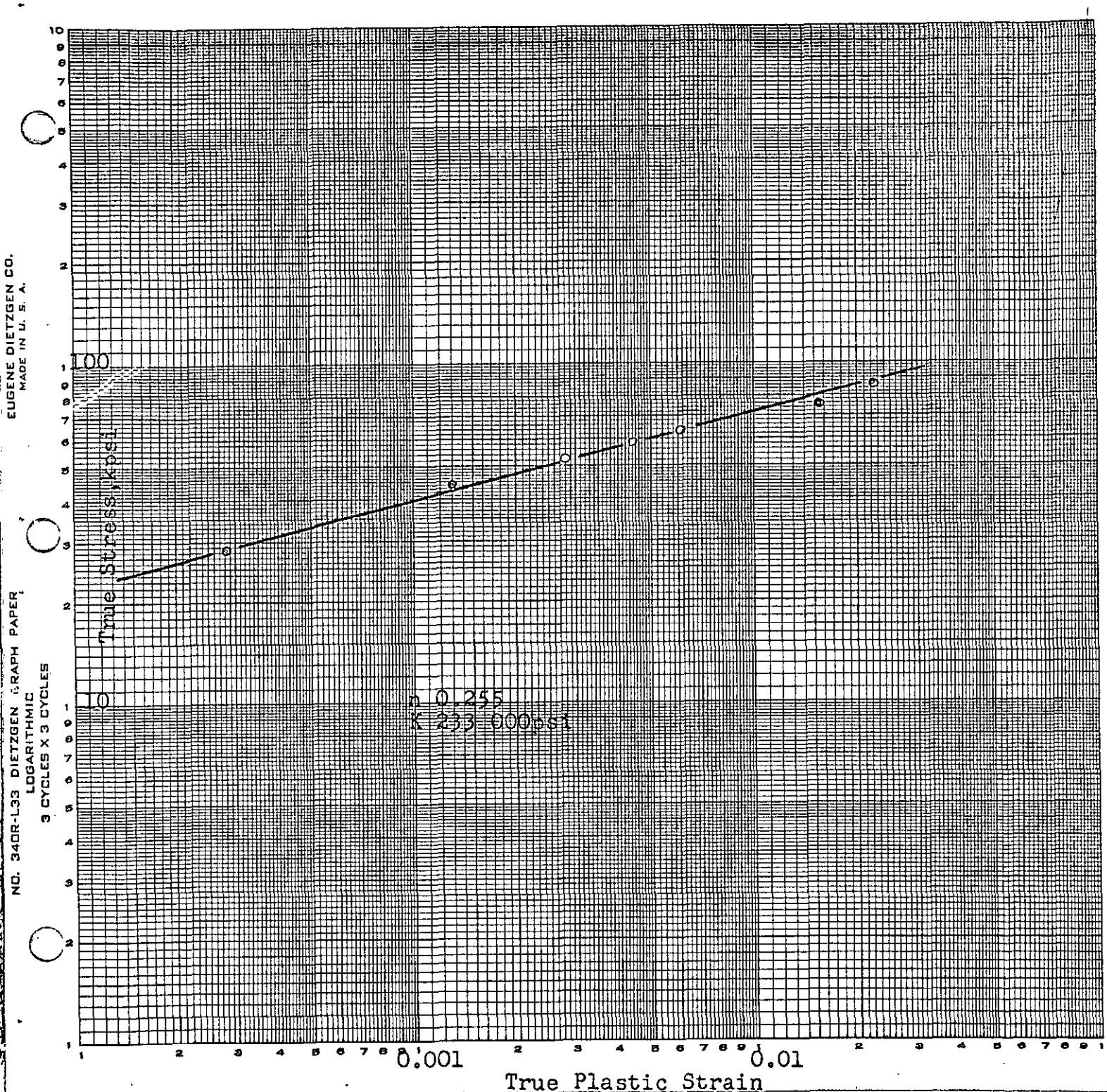

FIGURE 12. TRUE STRESS-TRUE STRAIN BEHAVIOR OF ALLOY 98464
U-287 ppm Fe-361 ppm Si-<6 ppm Al

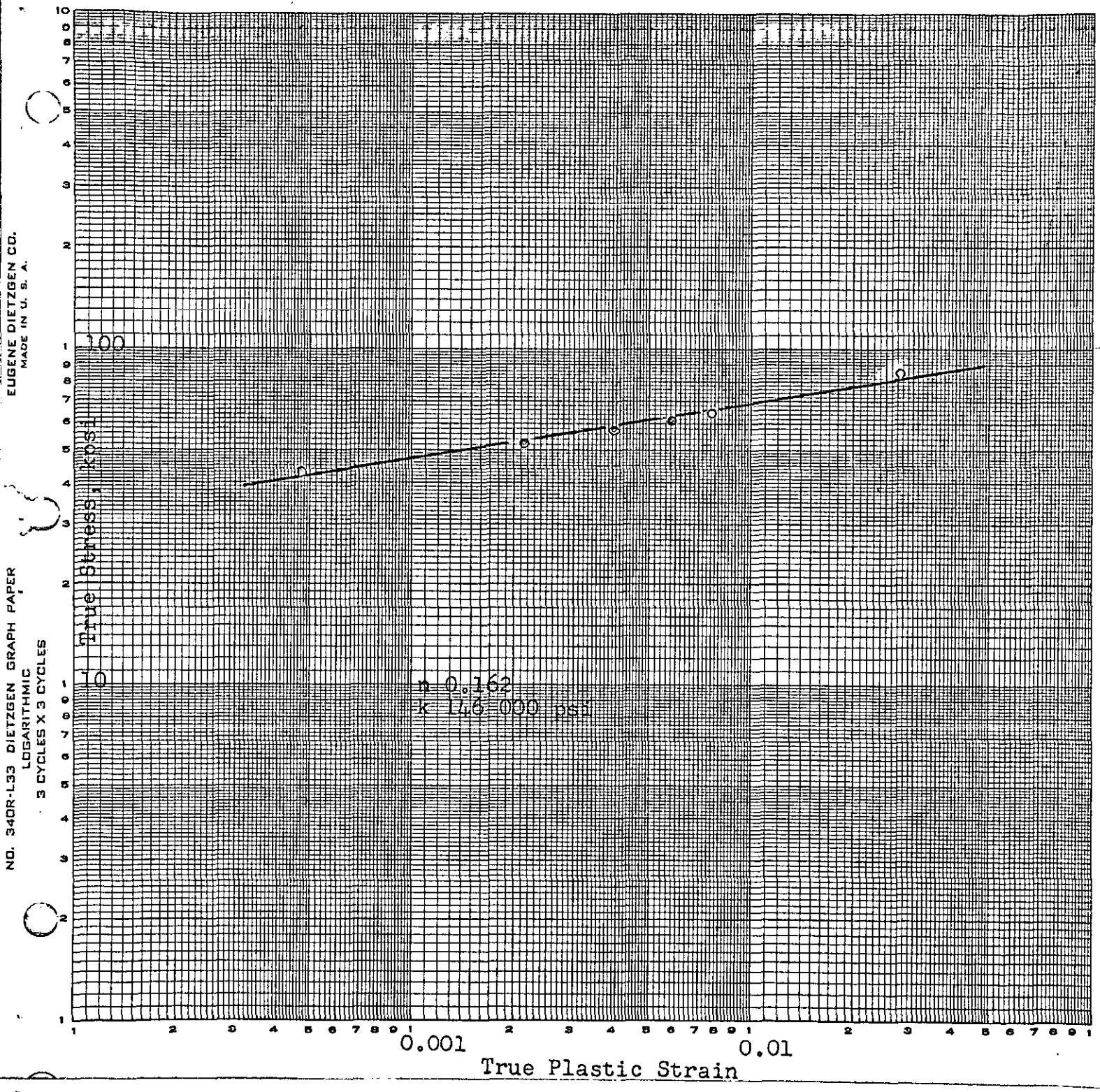

FIGURE 13. TRUE STRESS-TRUE STRAIN BEHAVIOR OF ALLOY 98483
U-63 ppm Fe-310 ppm Si-778 ppm Al

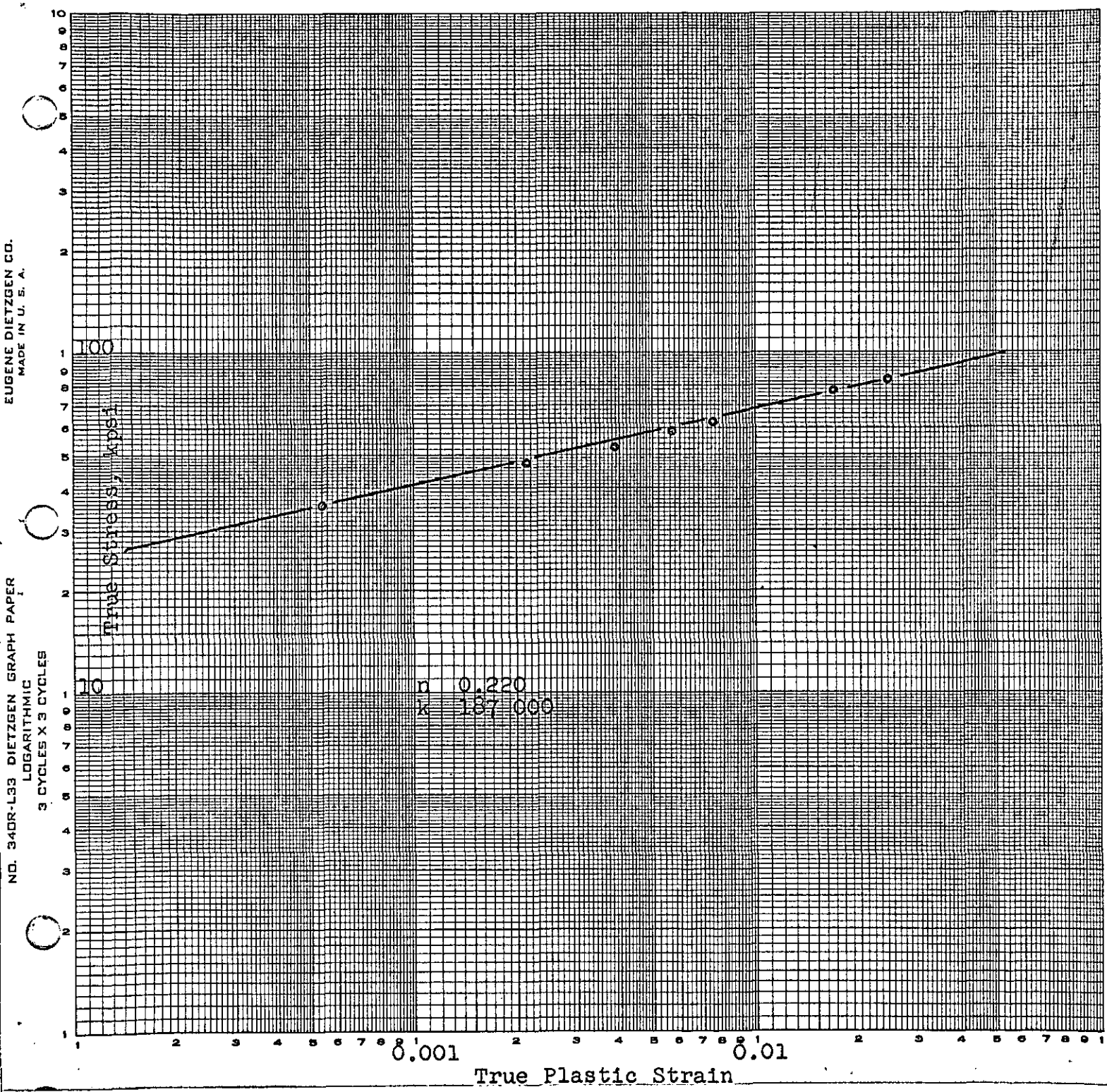

FIGURE 14. TRUE STRESS-TRUE STRAIN BEHAVIOR OF ALLOY 98470
U-75 ppm Fe-325 ppm Si-<6 ppm Al

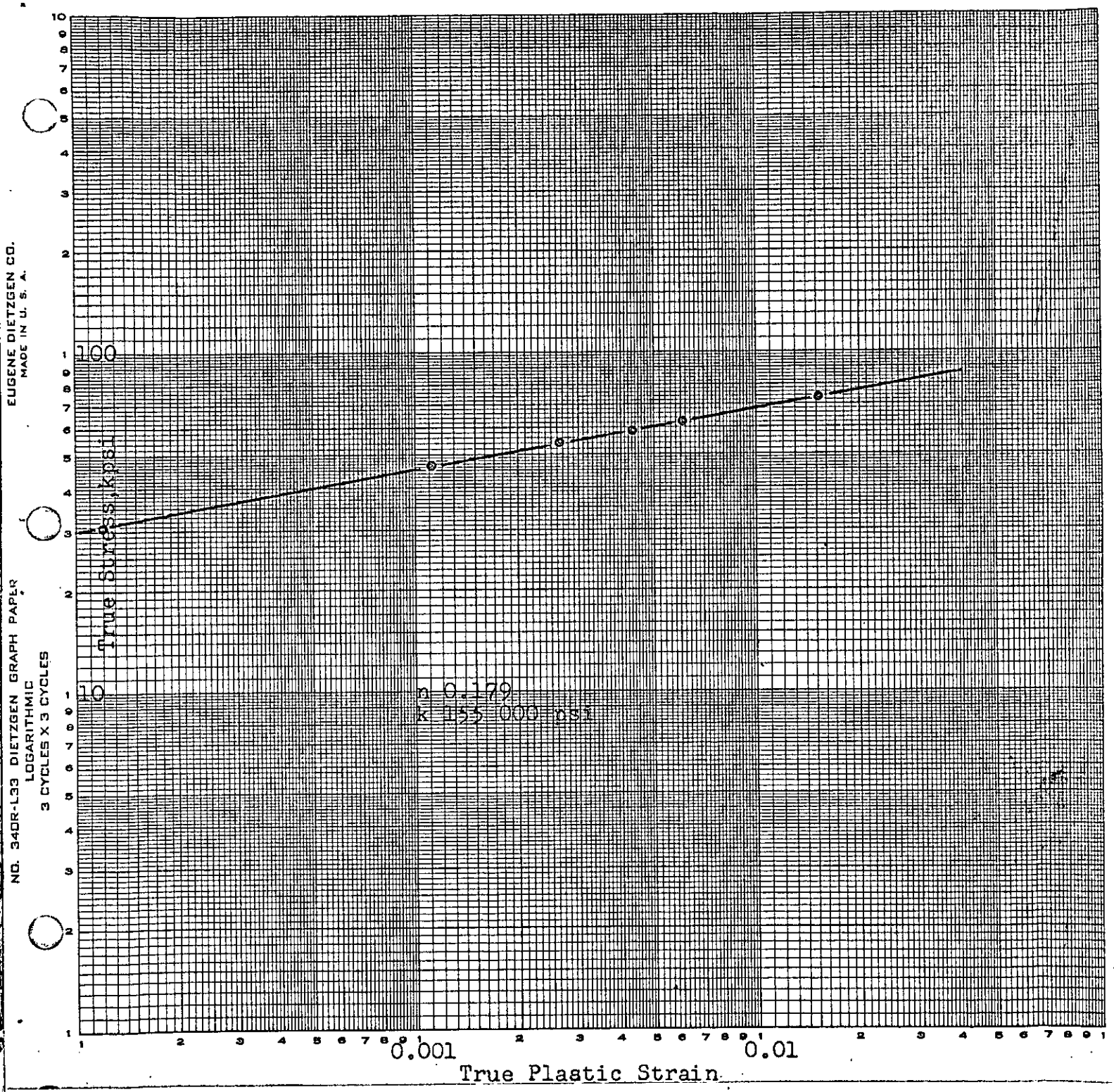

FIGURE 15. TRUE STRESS-TRUE STRAIN BEHAVIOR OF ALLOY 98479
U-289 ppm Fe-222 ppm Si-274 ppm Al

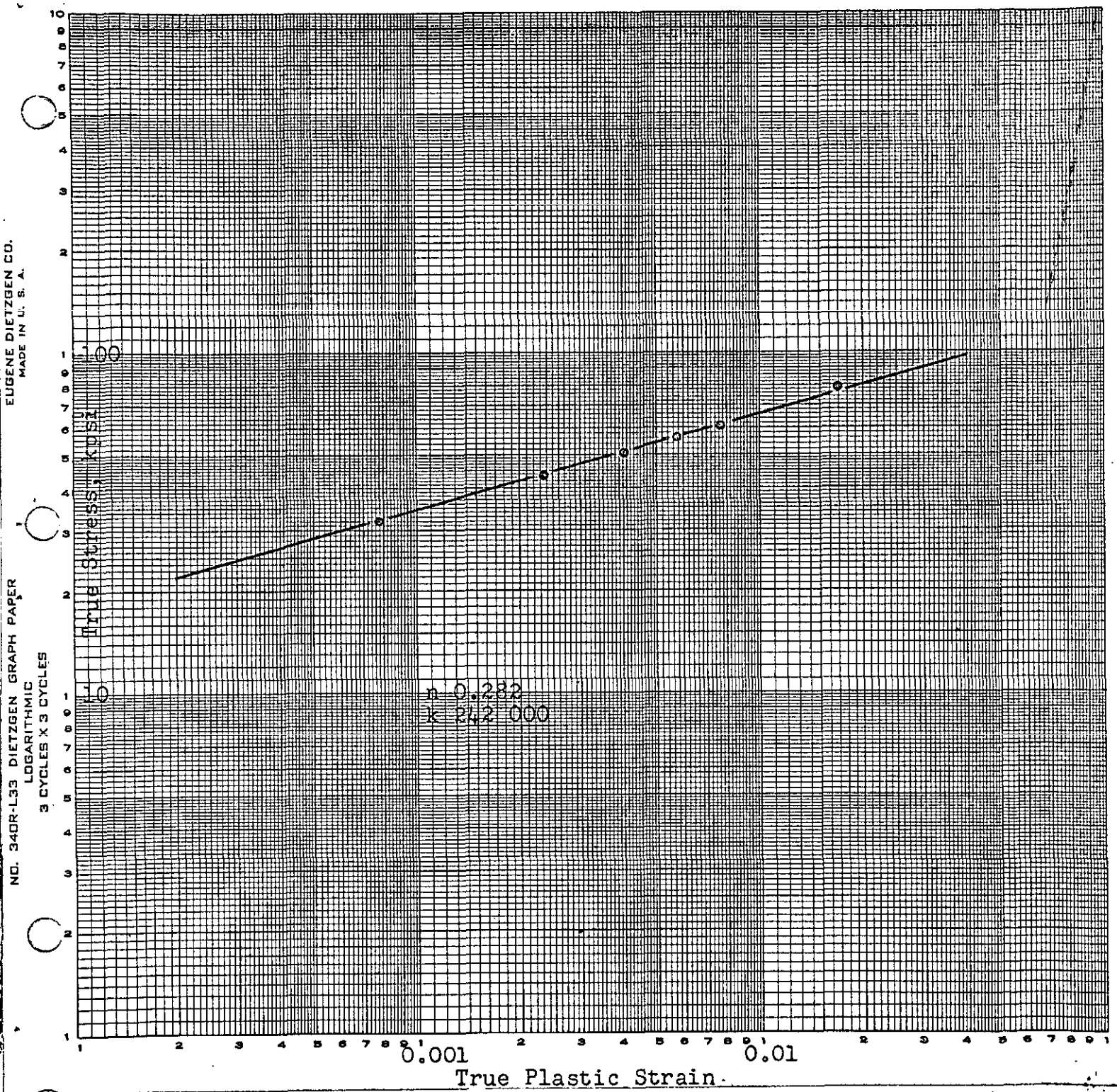

FIGURE 16. TRUE STRESS-TRUE STRAIN BEHAVIOR OF ALLOY 98727
U-98 ppm Fe-327 ppm Si-<6 ppm Al-1000 ppm Mo

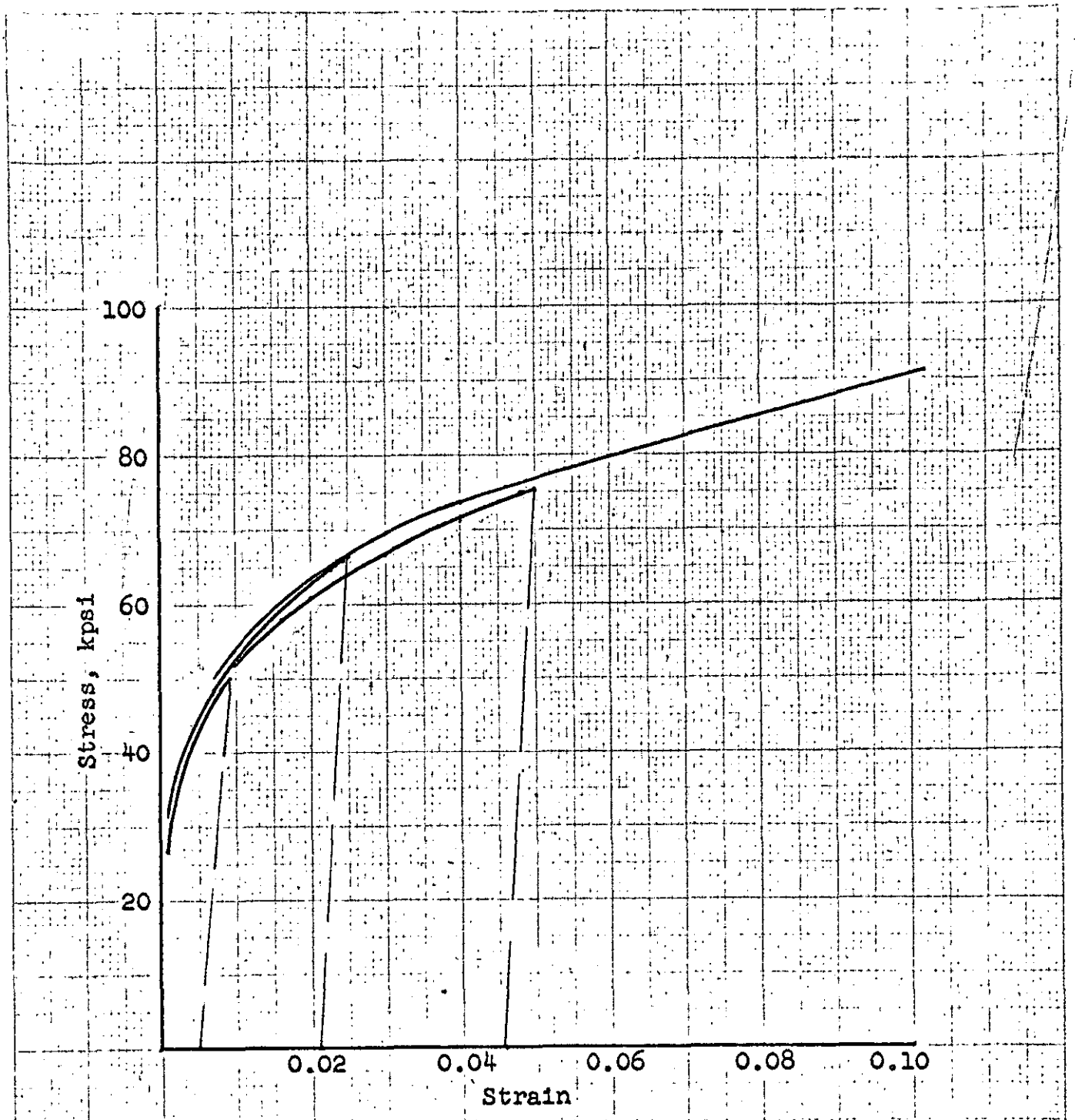

FIGURE 17. STRESS-STRAIN CURVES FOR UNALLOYED DINGOT URANIUM

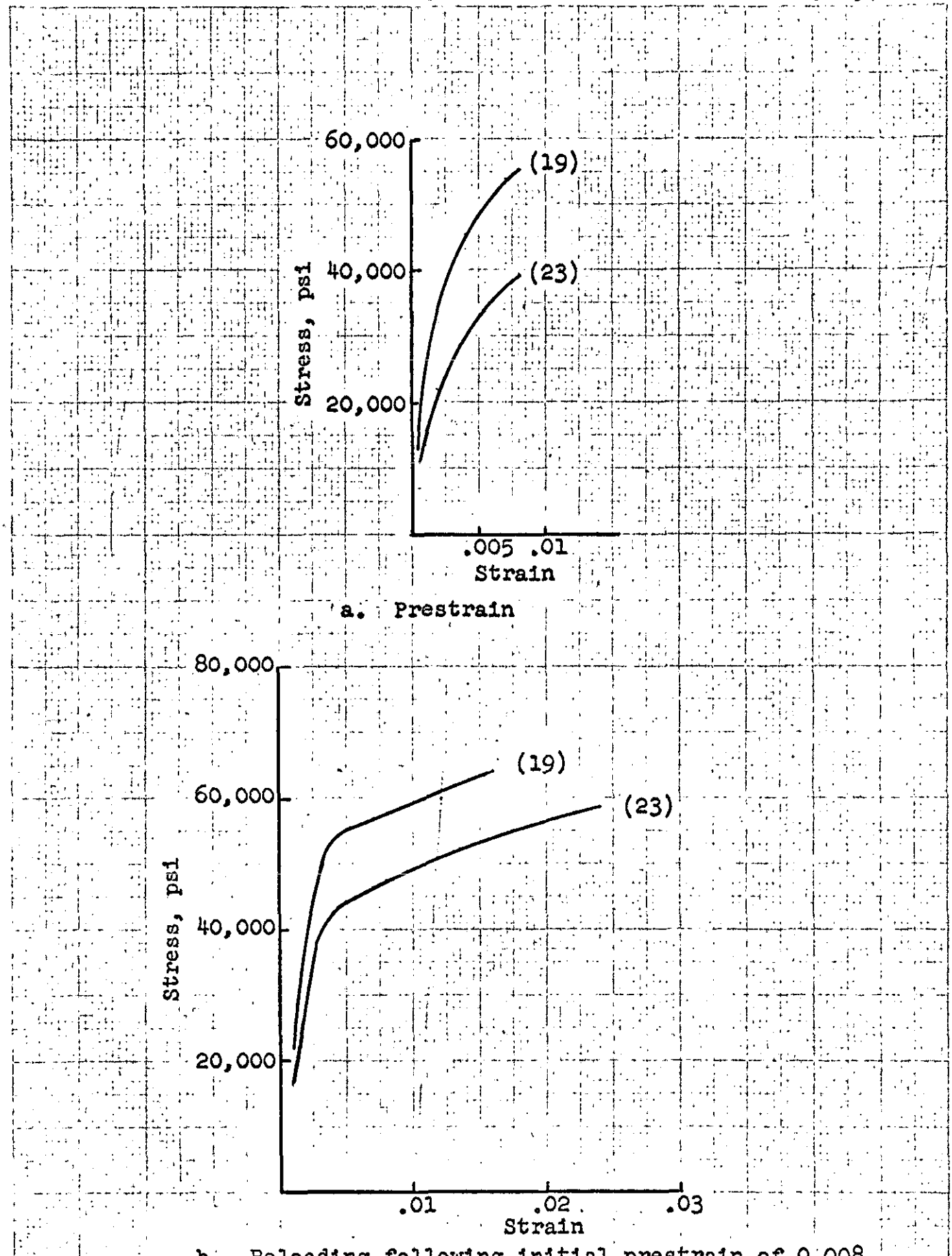

FIGURE 18. COMPARISON OF TENSILE CURVES FOR AS-MACHINED (19) AND ANNEALED (23) SPECIMENS OF UNALLOYED URANIUM

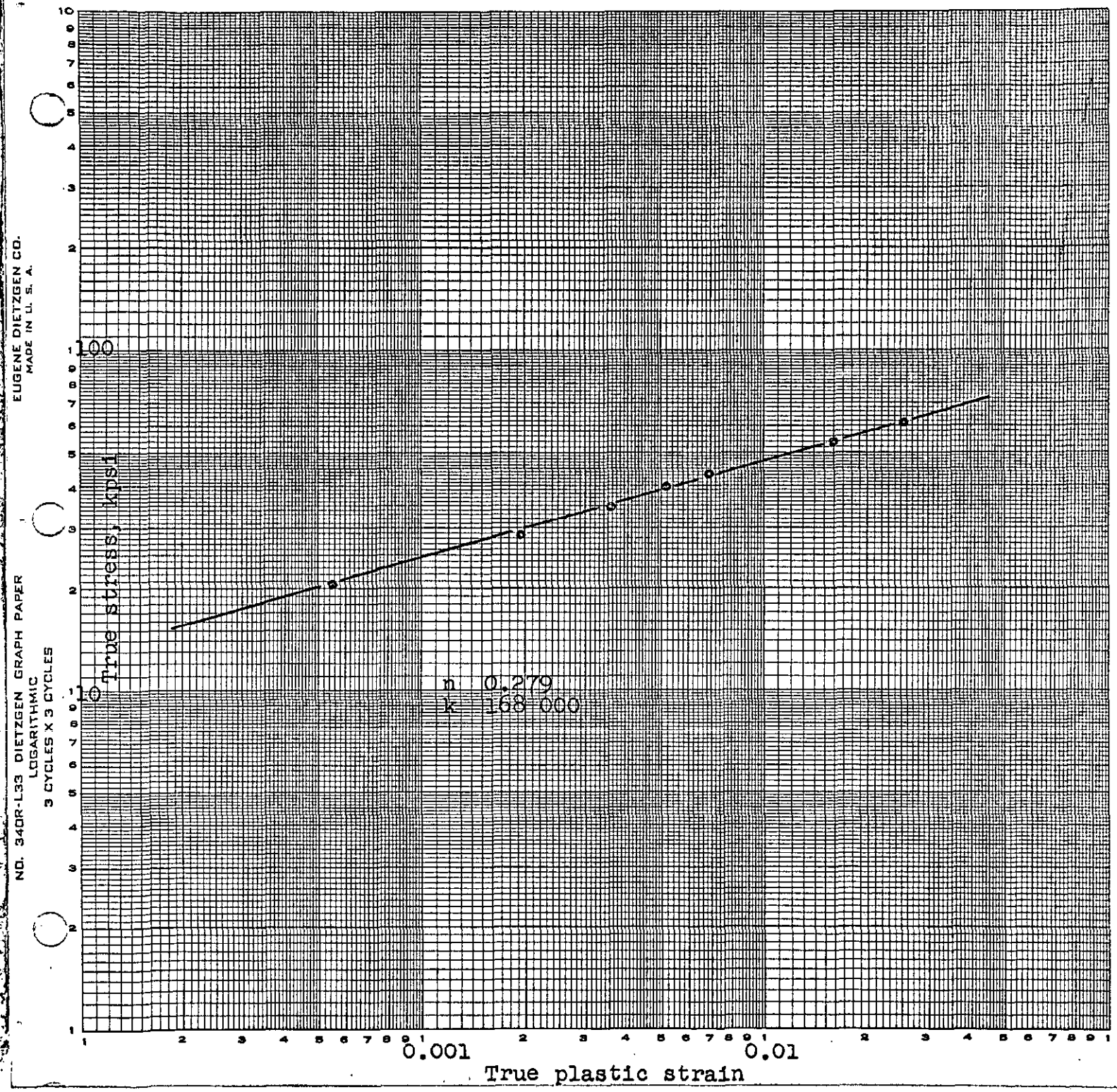

FIGURE 19. TRUE STRESS-TRUE STRAIN BEHAVIOR OF UNALLOYED DINGOT 993, ALPHA ANNEALED. U-57 ppm Fe-11 ppm Si-32 ppm Al

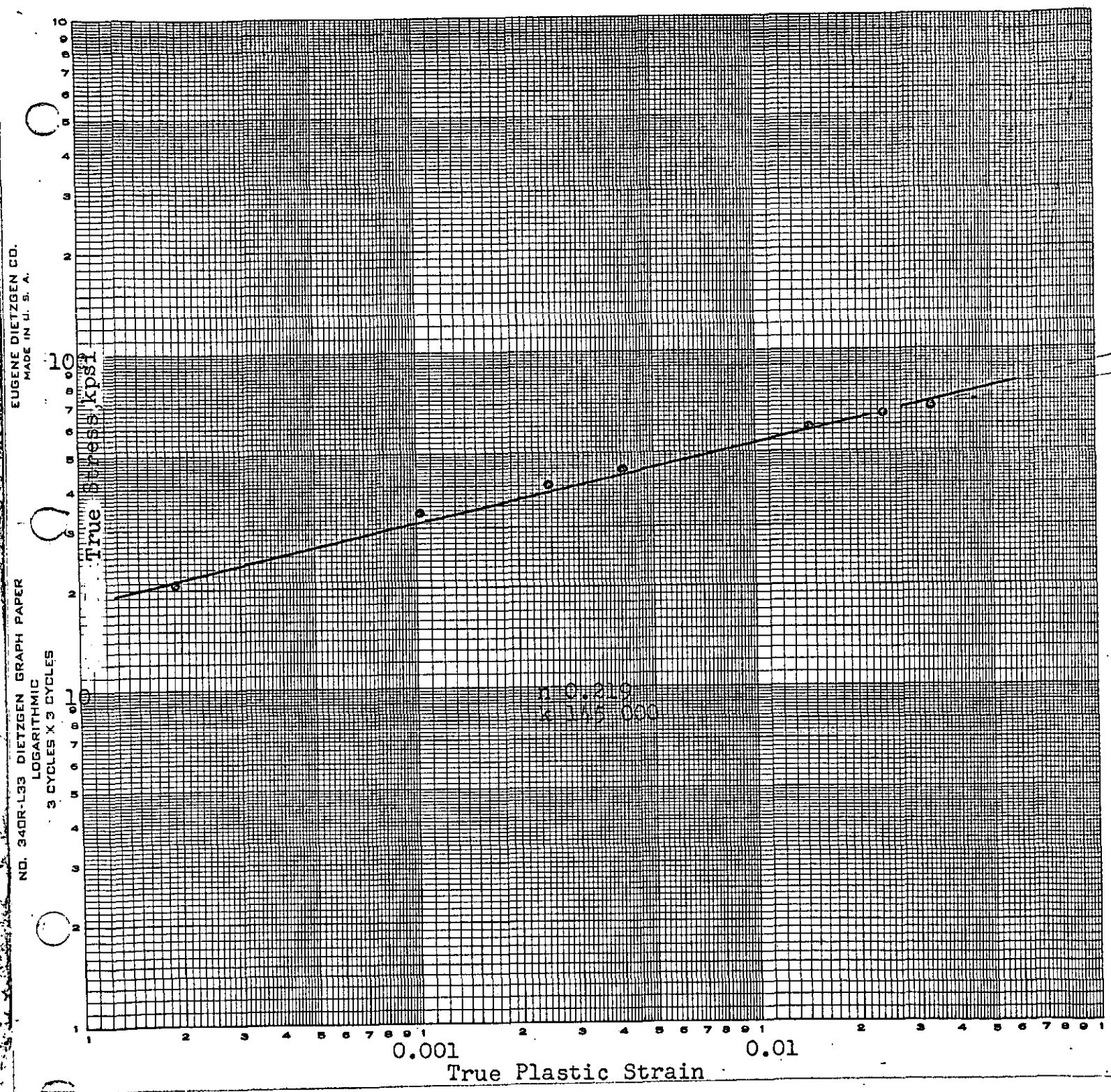

FIGURE 20. TRUE STRESS-TRUE STRAIN BEHAVIOR OF DINGOT 927(AB-1) U-150 ppm Fe-110 ppm Si-24 ppm Al

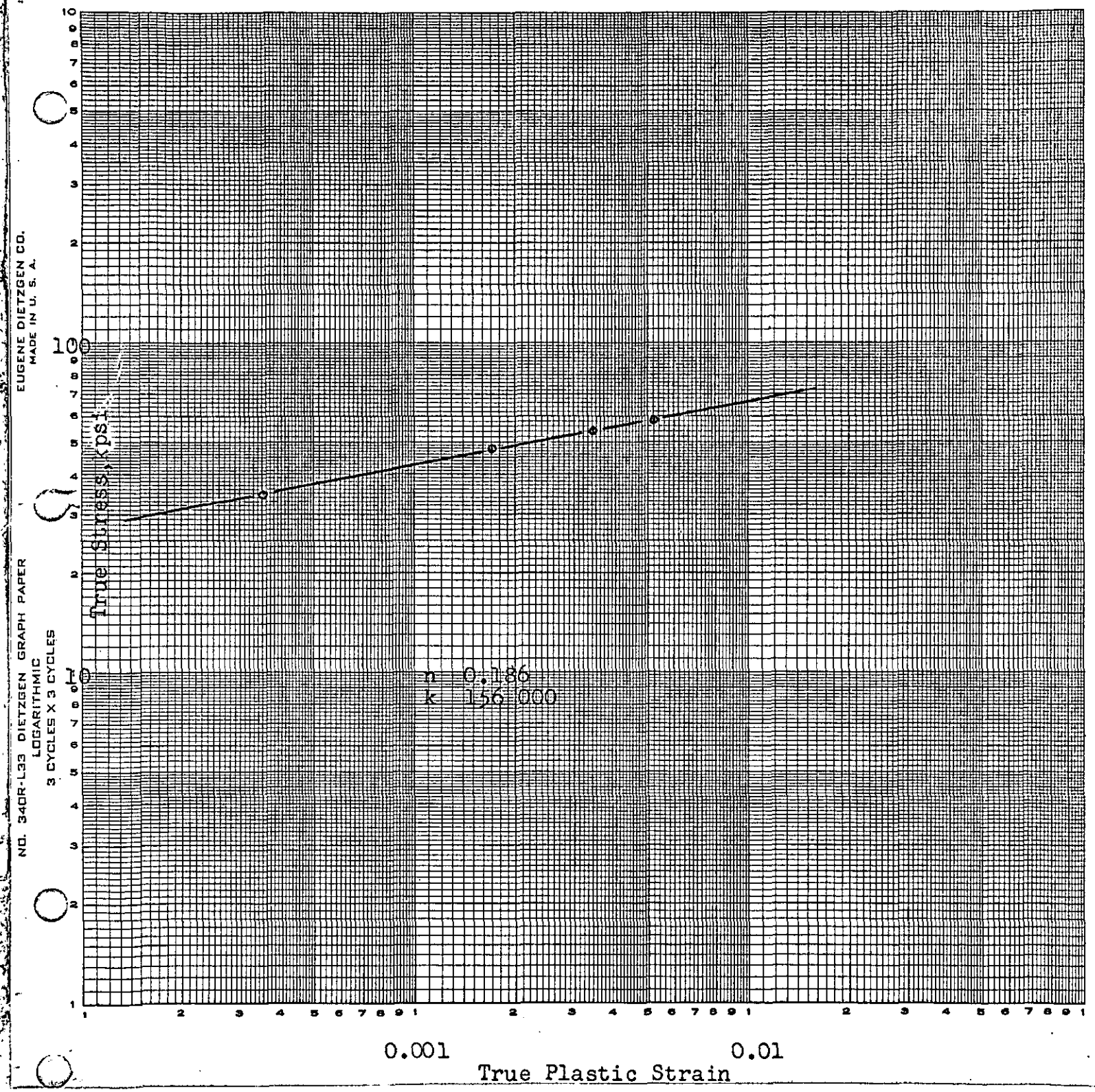

FIGURE 21. TRUE STRESS-TRUE STRAIN BEHAVIOR OF INGOT 92794, ALPHA ANNEALED. U-97 ppm Fe-39 ppm Si-16 ppm Al

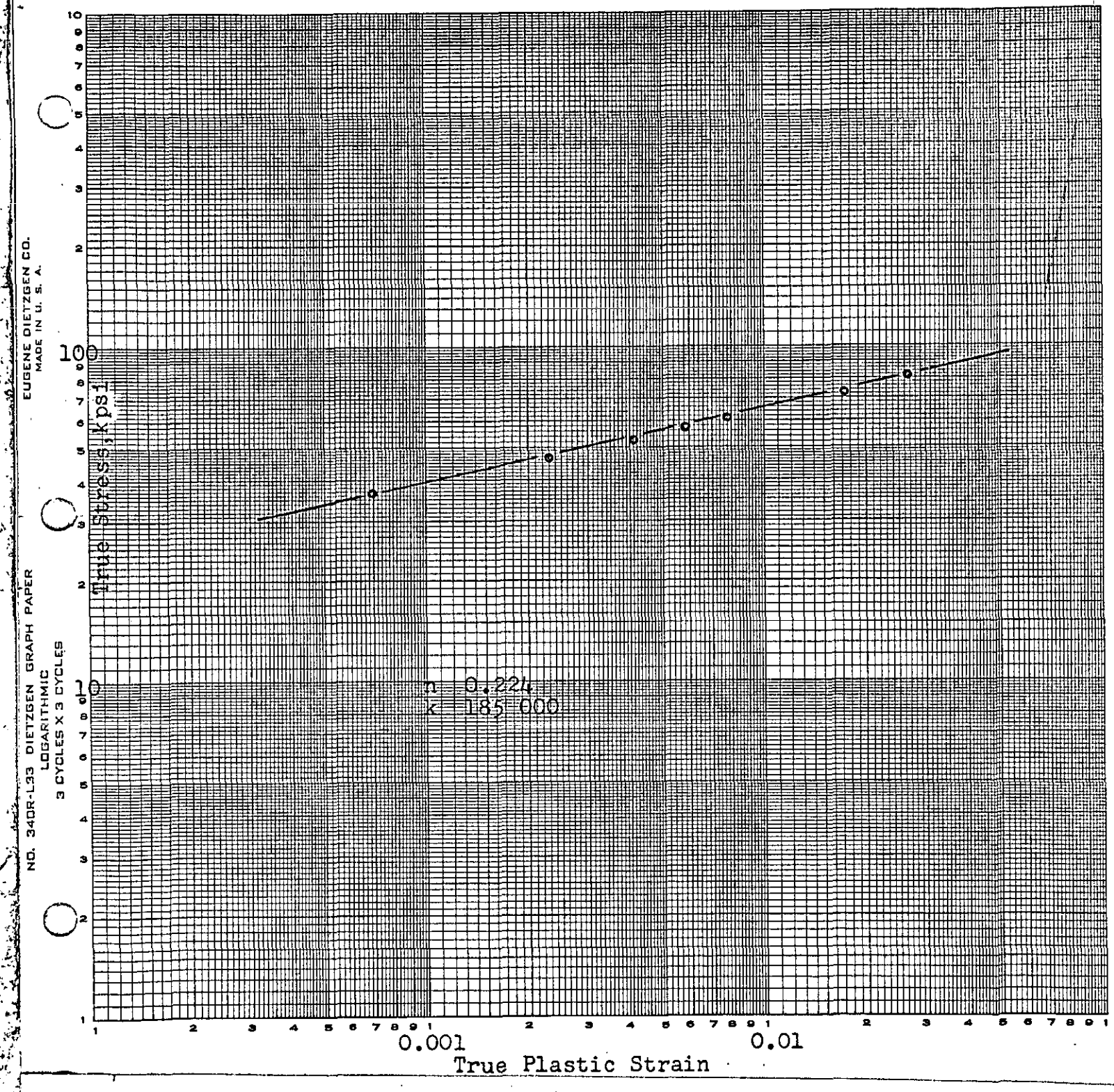

FIGURE 22. TRUE STRESS-TRUE STRAIN BEHAVIOR OF INGOT 92754, ALPHA ANNEALED. U-128 ppm Fe-58 ppm Si-7 ppm Al

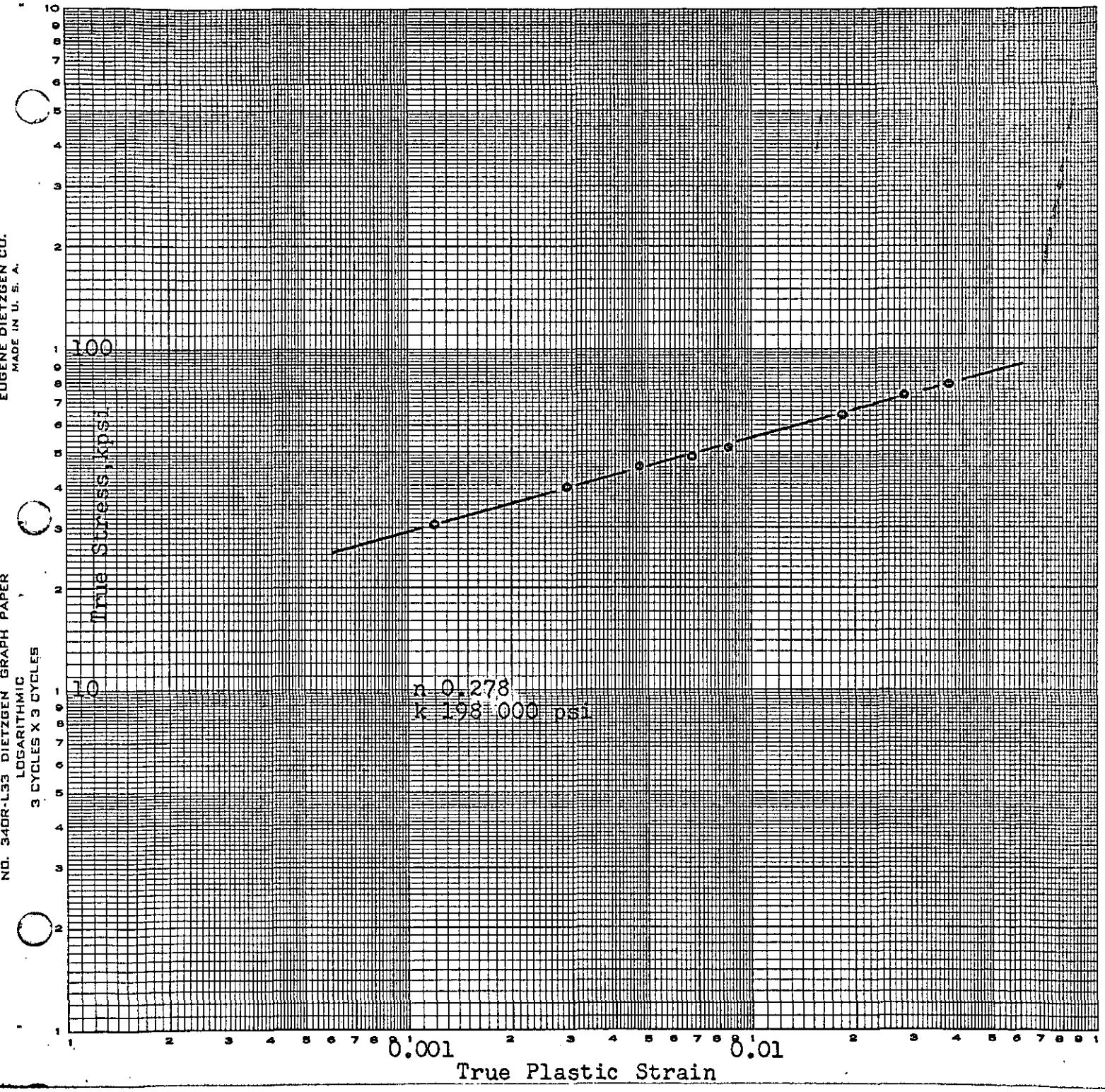

FIGURE 23. TRUE STRESS-TRUE STRAIN BEHAVIOR OF INGOT 33384, ALPHA ANNEALED. U-137 ppm Fe-88 ppm Si-<6 ppm Al

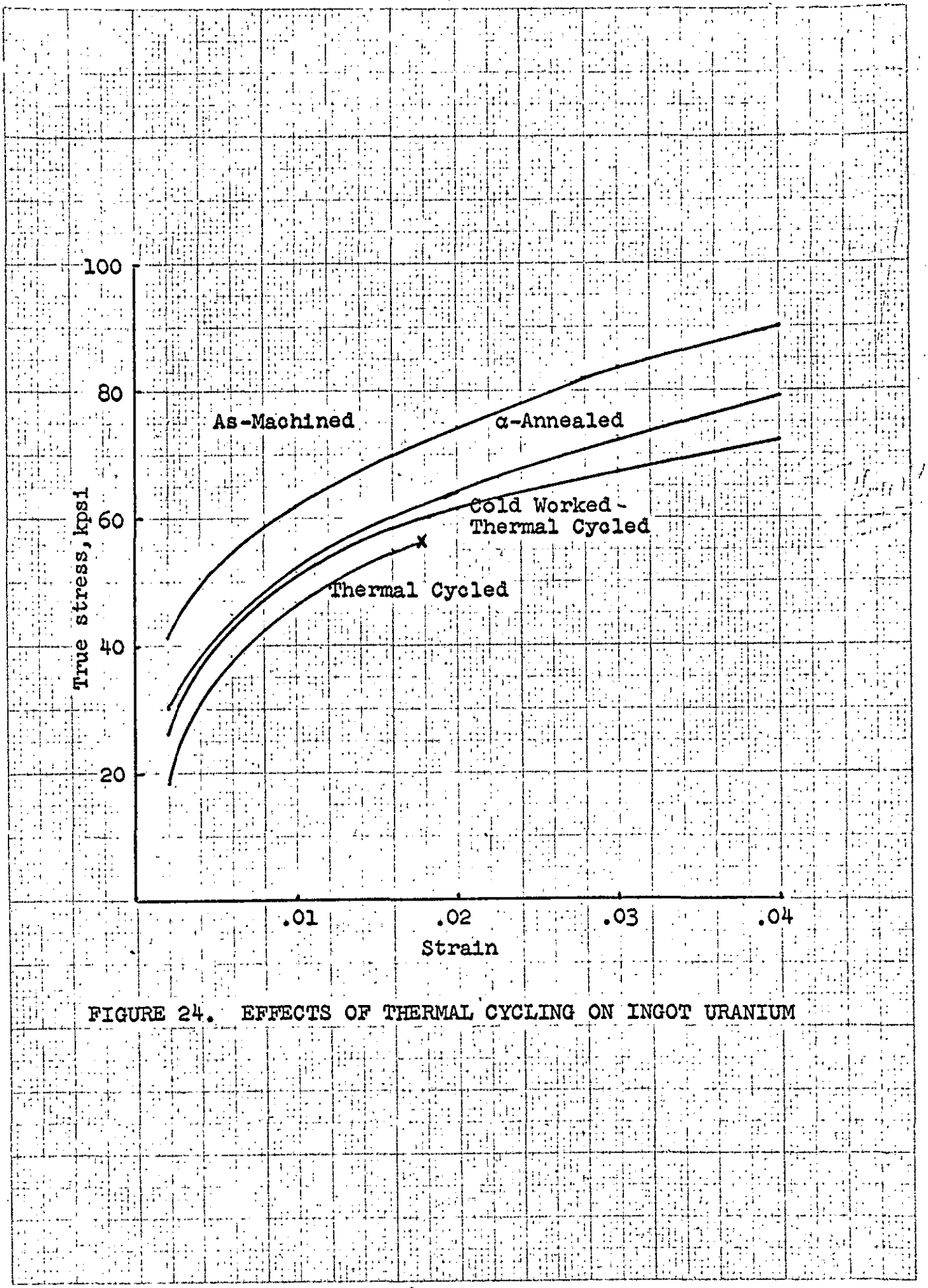

FIGURE 24. EFFECTS OF THERMAL CYCLING ON INGOT URANIUM

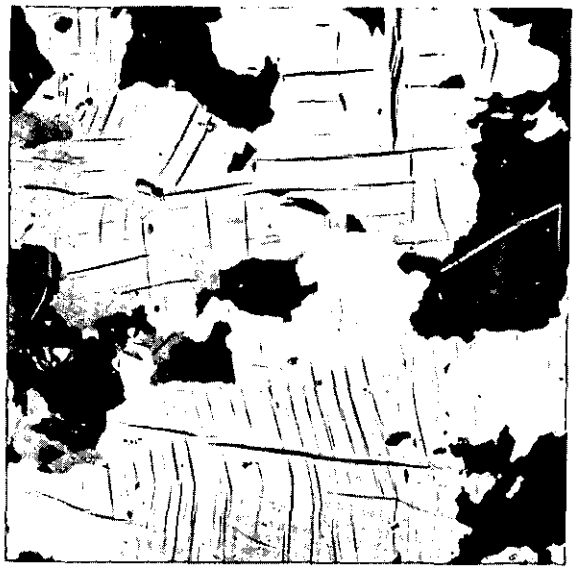

Neg. 55454

a. Specimen strained 0.9%.

Neg. 55457

b. Specimen strained 2.5%.

Neg. 55460

c. Specimen strained 5%.

Neg. 58572

d. Specimen strained 10.5%. Fractured.

FIGURE 25. VARIATION IN MICROSTRUCTURE OF UNALLOYED URANIUM WITH ROOM-TEMPERATURE TENSILE DEFORMATION (150X)

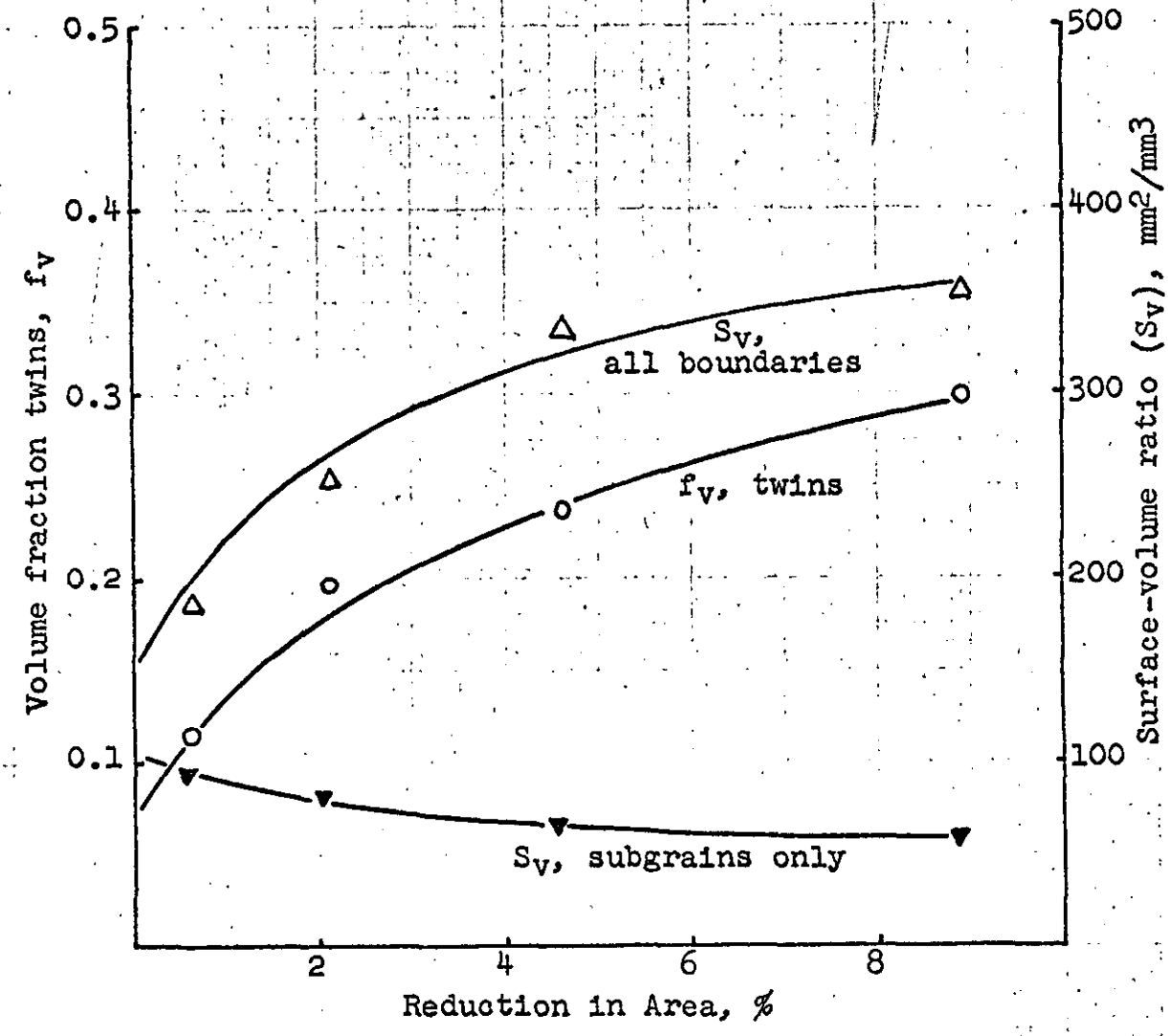

Unalloyed dingot uranium in the beta, oil-quenched condition.

FIGURE 26. RELATION OF TWINNING AND INTERNAL BOUNDARY AREA TO DEFORMATION IN DINGOT URANIUM

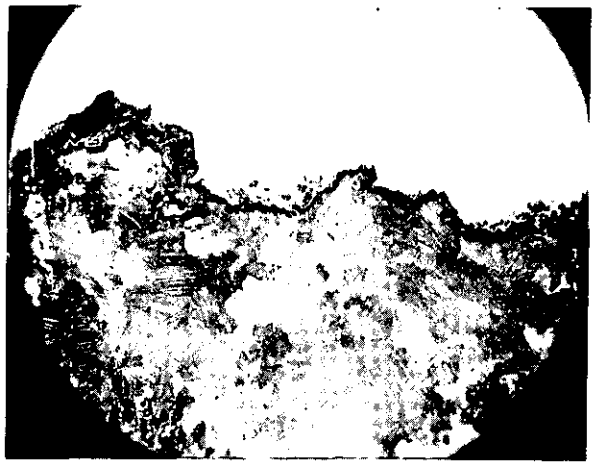

Neg. 62830 25X

a. Unalloyed ingot uranium, 33382. Ragged fracture typical of most specimens.

Neg. 62832 150X

b. Grain boundary crack in same specimen, 1/2 inch from principal fracture.

FIGURE 27. FRACTURES IN INGOT URANIUM TENSILE SPECIMENS

Neg. 62851 150X

U-300 ppm Si-800 ppm Al alloy (XD2). Secondary crack is surrounded by heavily twinned metal.

FIGURE 28. SECONDARY CRACK PERPENDICULAR TO MAIN FRACTURE

Neg. 58558 6X

a. Double fracture in dingot uranium.

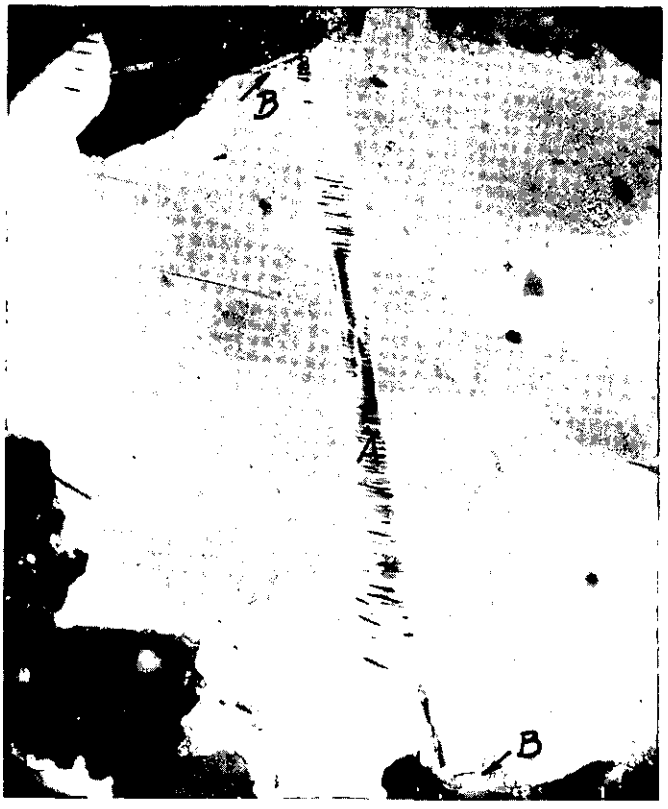

Neg. 58563 250X

b. Kink band (A) with grain boundary cracks (B) at both ends. Tension axis vertical.

FIGURE 29. DOUBLE FRACTURE AND DEFORMATION KINK, DINGOT URANIUM 993

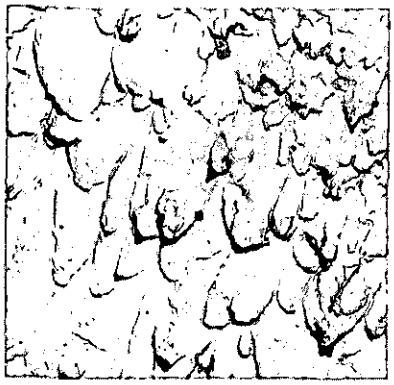

1859E 5800X
Dingot 2122

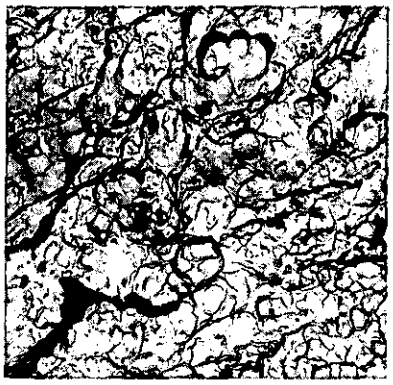

1855D 5800X
Dingot 3260

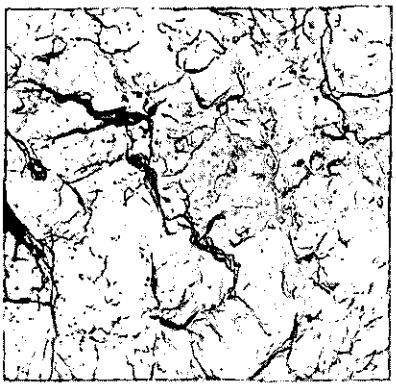

1928B 4200X
Ingot 98727

a. Fibrous fracture surfaces, characteristic of ductile fracture.

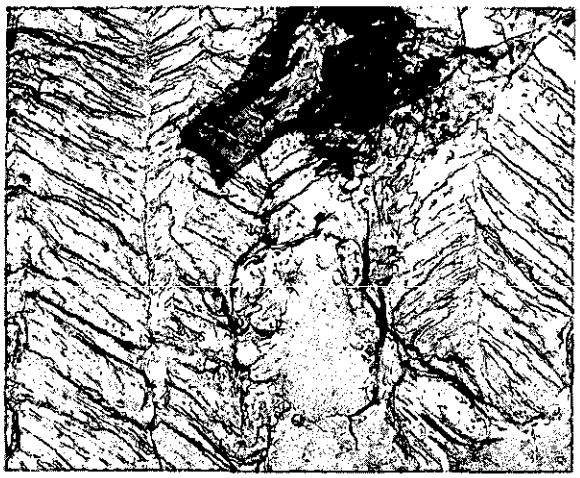

1855A 5800X

Dingot 3260

b. Stair-step cleavage, low ductility fracture.

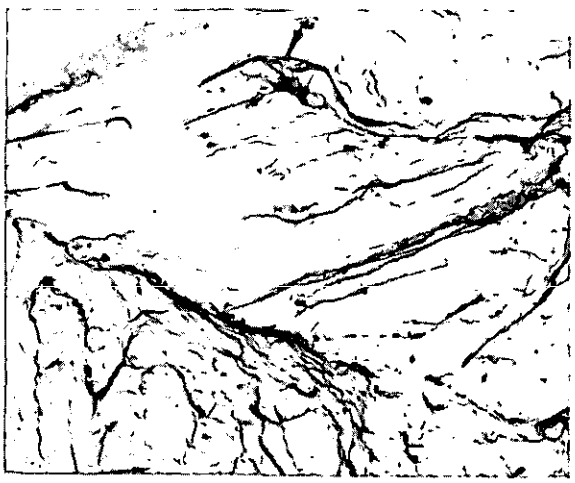

1672I 11,100X

Ingot 98359

c. "River" patterns characteristic of cleavage, low ductility fracture, Note change in fracture characteristics at grain boundary.

FIGURE 30. TYPICAL FRACTURE SURFACES OF URANIUM ALLOYS BROKEN AT ROOM TEMPERATURE

Neg. 1926B 5700X

a. Photomicrograph showing fracture initiation point in ingot 98359.

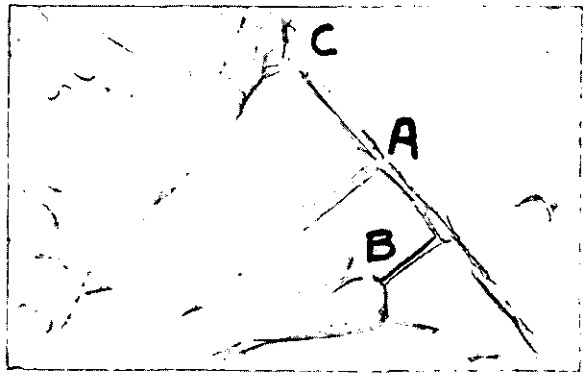

Neg. 1926A 12,500X

b. Enlargement of Figure a showing cracking due to twin-twin intersection (A), twin-second phase intersection (B), and twin-grain boundary intersection (C).

FIGURE 31. FRACTURE INITIATION IN URANIUM ALLOYS